

Simulation and Test of a Cooling Cycle for the PENeLOPE Experiment

Simulation und Test eines Kühlzyklusses für das PENeLOPE Experiment

Oliver Schurius

Institute for Hadronic Structure and Fundamental Symmetries (E18)
Physik-Department Technische Universität München

Wissenschaftliche Arbeit zur Erlangung des Grades

Bachelor of Science

an der Fakultät für Physik der Technischen Universität München.

Themensteller

Prof. Dr. Stephan Paul

Zweitgutachter

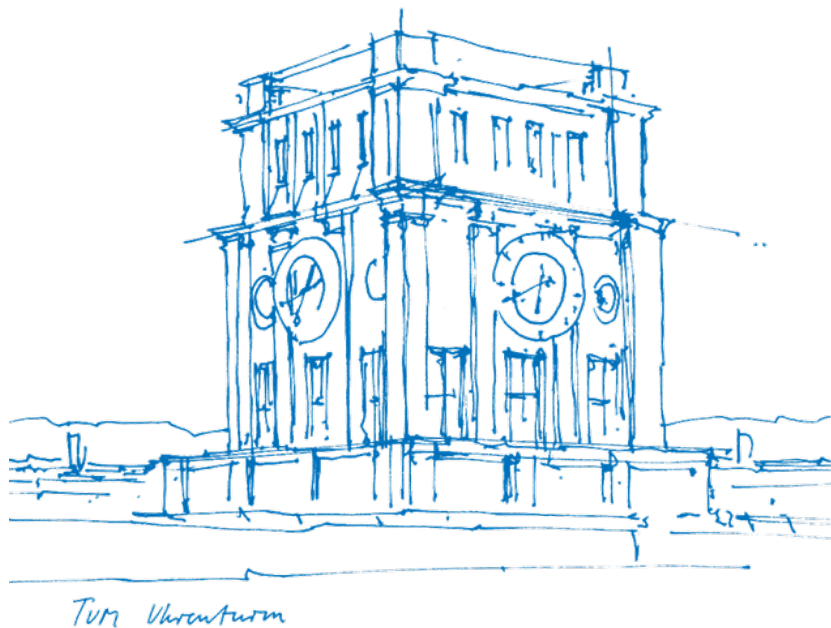
Prof. Dr. Bruno Leibundgut

Betreut von

Rainer Stoepler

Eingereicht am

München, den 14.10.2020



Abstract

For the magnets of PENeLOPE to obtain a field strength of up to 5.5 T, they need to reach the superconducting phase. The critical temperature for the Niobium–titanium (NbTi) superconductor used in the PENeLOPE experiment is about 10 K [1].

Liquid helium ($T \lesssim 4.2\text{ K}$) is used as a direct coolant on the coils, while liquid nitrogen ($T \lesssim 77.3\text{ K}$) - along with multiple insulations - serve as a shield from the external heat. Because of the high cost for helium especially, it is imperative to make the cooling process as efficient as possible while keeping the cooling time reasonable.

After a short overview of the theory of heat transfer, the assembly of PENeLOPE is demonstrated. Then, the simulation of the cooling cycle is thoroughly explained. Finally, the results of the simulation are analyzed and compared to the measurements before a conclusion is drawn.

Unfortunately, it was not yet possible to use liquid helium in the cooling process of the magnet as of the writing of this. Therefore, all comparisons of the simulation results and the measurements only involve the cooling with liquid nitrogen, which will therefore be the focus of this thesis.

Contents

1	Introduction	5
2	General method & formulas	6
2.1	Thermal conduction	6
2.2	Convective heat transfer	6
2.3	Thermal radiation and Multi-layer Insulation	7
2.4	Specific heat capacity	10
3	General assembly of PENeLOPE	11
3.1	The magneto-gravitational trap	12
3.2	The helium tank	14
3.3	The nitrogen shield	15
3.4	The outer wall and lid	16
4	Simulation with Simulink®	17
4.1	Used blocks in the Simulink® simulation	18
4.2	Remarks on the simulation and overview	21
4.3	Simulation involving the nitrogen shield	24
4.4	Simulation of the heat flow in and to the helium tank	30
5	Simulation results, comparison to measurements & discussion	36
5.1	Results without helium	37
5.1.1	Determining the cooling time for a continuous nitrogen flow	38
5.1.2	Comparison of simulation results and measurements	40
5.2	Results with helium	42

5.2.1	Magnet temperature using only helium	43
5.2.2	Magnet temperature using helium and nitrogen	44
6	Conclusion and outlook	47
Appendices		48
A	Calculation of the magnet mass	48
B	Example simulations to demonstrate the influence of the isolation vaccum and the inclusion of MLI	48
C	Non-simplified simulation involving only liquid nitrogen	49
D	Justification for only examining the simplified simulation	50
E	Dimensions of components as used in the simulation	51
F	Calculation of the liquid level necessary to cover the quench protection	53
G	Sensor descriptions	55
H	Liquid level in the case of an insufficient helium flow rate	56
I	Calculation of the helium mass needed to cool down the magnet under ideal circumstances	56

1 Introduction

Inside an atomic nucleus, a typical neutron can survive for a very long time and may even never decay, but on its own, it will transform into other particles within 15 minutes, more or less. The words “more or less” cover a disturbing gap in physicists’ understanding of this particle. Try as we might, we have not been able to accurately measure the neutron lifetime.

-Geoffrey L. Greene, Peter Geltenbort [2]

The neutron lifetime τ_n has been puzzling scientists for decades. The two types of precision experiments (in-beam and storage) disagree on the lifetime of the free neutron. But a clear picture of the behaviour of this particle is crucial for understanding the nature of the universe. Since the neutron decay is one of the most simple examples of the weak nuclear interaction, it is necessary to know how long neutrons live to truly understand the weak force. Apart from that, the ratio of hydrogen to heavier nuclei in the universe is dependent on the neutron lifetime. At this point in time, the value of τ_n contributes the largest uncertainty in theoretical calculations of the primordial ^4He abundance from Big Bang Nucleosynthesis [3]. One potential way to resolve the neutron lifetime enigma is to carry out new types of experiments that do not share the same kind of systematic uncertainties to past ones. This is where PENeLOPE (Precision Experiment on Neutron Lifetime Operating with Proton Extraction) comes in.

What makes PENeLOPE distinct from most other neutron lifetime measurements is the use of a magneto-gravitational trap. This means that - in the vertical direction - neutrons are bound by gravity alone, allowing for placement of a proton detector directly on top of the storage volume. In contrast to other storage type experiments, PENeLOPE can therefore provide a direct measurement of the neutron decay rate along with the count of remaining neutrons after certain storage times, allowing for a more accurate control of the systematic uncertainties. PENeLOPE has an error margin goal of 0.1 s or less, which is an order of magnitude smaller than all previous neutron lifetime experiments [4].

2 General method & formulas

2.1 Thermal conduction

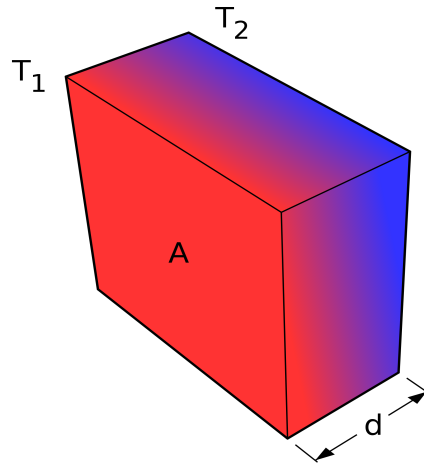


Fig. 1: Heat flow through a wall with thickness d and area A connected to temperatures T_1 and T_2 [5]

Thermal conduction describes the transport of heat through a material (see figure 1). The heat power flowing through a solid with two parallel walls is determined by Fourier's law:

$$\dot{Q} = \lambda(T) \cdot A \cdot \frac{T_1 - T_2}{d} \propto \Delta T. \quad (1)$$

Here, $\lambda(T)$ is the thermal conductivity of the material.

In isolators, thermal conduction is carried solely due to lattice vibrations (phonons), meaning that movement of an atom is passed to its neighbours through collisions. (Semi-)conductors however contain free electrons that can contribute to thermal conduction. For conductors like metals, this effect actually outweighs the conductivity due to phonons.

2.2 Convective heat transfer

Convective heat transfer, or simply convection, is the transfer of heat by way of movement of fluids. There are two types of convection: Natural and forced. In natural convection, fluid motion is caused by natural means such as the buoyancy effect arising from temperature differences among fluid molecules or among a contacting surface and the fluid. Forced

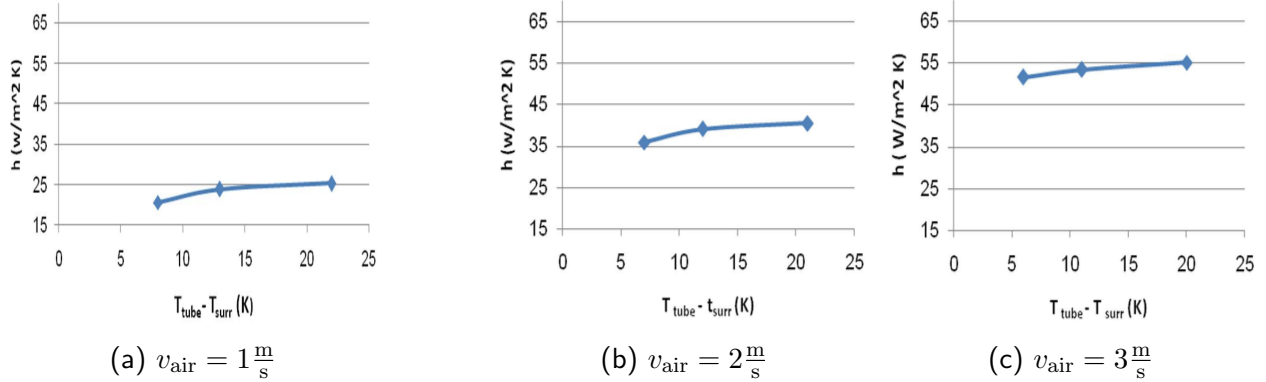


Fig. 2: Convective heat transfer coefficient $h(T)$ between aluminum metal finned tubes and air for different air velocities (forced convection). As you can see, it is strongly connected to the behaviour of the fluid [7].

convection arises when there is an external force such as a pump or fan driving the fluid over a surface such as a tube [6].

In a very simplified model, convection can be described by Newton's law of cooling. It states that the heat loss of a body is proportional to the temperature difference between it and its surroundings and scales linearly with the surface area:

$$\dot{Q} = h(T) \cdot A \cdot (T_{\text{body}} - T_{\text{surr}}) \propto \Delta T. \quad (2)$$

Here, $h(T)$ denotes the convective heat transfer coefficient. This value is strongly dependend on the roughness of the solid surface and the fluid properties as well as the type of flow (laminar or turbulent). Figure 2 shows the convective heat transfer coefficient between air and aluminum finned tubes over the temperature difference for different air velocities.

2.3 Thermal radiation and Multi-layer Insulation

As oppose to thermal conduction and convection, thermal radiation does not require a transport material, since it is carried by electromagnetic radiation (photons). In a vacuum, it is the only form of heat transport.

Every material gives off radiation that has a maximum intensity at a different wavelength λ_{max} depending on the temperature. A black body describes an idealized thermal body that absorbs all incident electromagnetic radiation, but (in thermal equilibrium) also emits energy according to the Planck Radiation law

$$I(\nu, T) = \frac{2h\nu^3}{c^2} \cdot \frac{1}{\exp\left(\frac{h\nu}{k_B T}\right) - 1}. \quad (3)$$

Here, I denotes the intensity of radiation with frequency ν in units of $\frac{\text{W}}{\text{m}^2\text{Hz}}$. For our purposes ($T \ll 5000\text{K}$), λ_{\max} is always in the infrared (see figure 3).

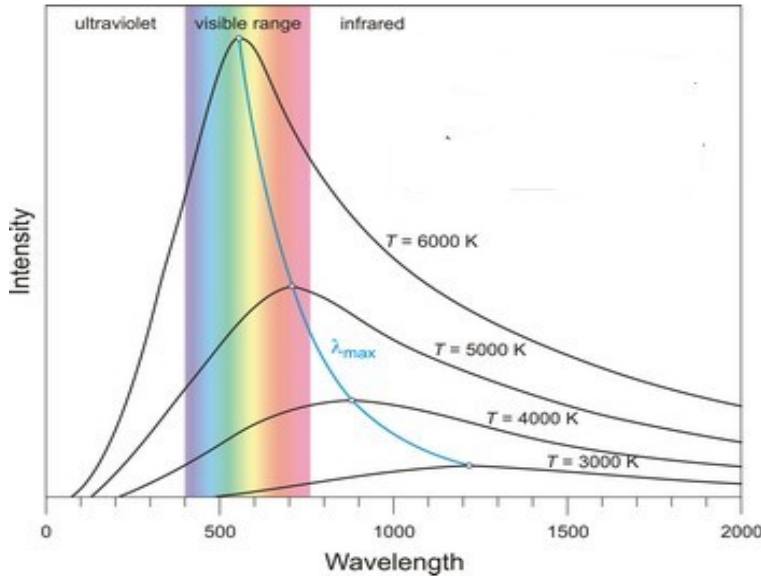


Fig. 3: Blackbody radiation for different temperatures. The blue line indicates the wavelength at which the radiation intensity is maximal [8]

To calculate the power radiated per unit area from a black body in terms of its temperature, the Stefan-Boltzmann law is used. It can be derived by integrating the intensity $I(\nu, T)$ over all frequencies ν and solid angles $d\Omega$. It yields

$$j = \frac{\dot{Q}}{A} = \sigma \cdot T^4, \quad (4)$$

with $\sigma = \frac{2\pi^5 k^4}{15c^2 h^3} \approx 5.67 \cdot 10^{-8} \frac{\text{W}}{\text{m}^2\text{K}^4}$ being the Stefan-Boltzmann constant. Real bodies do not absorb all incident radiation and therefore emit less total energy than a black body in thermal equilibrium. They are characterized by an emissivity $\epsilon < 1$ and the Stefan-Boltzmann law is modified to

$$j = \epsilon \cdot \sigma \cdot T^4. \quad (5)$$

Consequently, the heat flow between two bodies separated in a vacuum is

$$\dot{Q} = k \cdot A \cdot (T_A^4 - T_B^4), \quad (6)$$

where A is the emitting body surface area, T_A and T_B are the temperatures of the bodies and k is the radiation coefficient. Note the T^4 behaviour, resulting in a vastly different heat flow for different temperature gradients compared to thermal conduction and convection. The radiation coefficient k depends on the shapes, dimensions and emissivities of both the emitting and receiving body. For two parallel plates with emissivities ϵ_1 and ϵ_2 , the radiation coefficient is computed as

$$k_{\text{plates}} = \frac{\sigma}{\frac{1}{\epsilon_1} + \frac{1}{\epsilon_2} - 1}. \quad (7)$$

Similarly, the radiation coefficient for two concentric cylinders is equal to

$$k_{\text{cyl}} = \frac{\sigma}{\frac{1}{\epsilon_1} + \frac{1-\epsilon_2}{\epsilon_2} \frac{r_1}{r_2}}, \quad (8)$$

where ϵ_1 and r_1 stand for the emissivity and radius of the emitting cylinder, while ϵ_2 and r_2 denote the values for the receiving cylinder.

Multi-layer Insulation

Multi-layer Insulation (MLI) is a type of lightweight insulation consisting of multiple layers of thin plastic film, coated on the outside with an aluminized reflective material [9]. To explain its function, consider this example: A square meter of surface with an emissivity of 1 is held at 300K in empty space (with an apparent temperature of 3K). According to the Stefan-Boltzmann law, this surface will emit approximately 460 W. Now imagine a thin layer with emissivity 1 placed in front of the surface. When thermal equilibrium is reached, the 460 W this layer receives from the surface will be emitted to each side. Half of it will be radiated back to the surface, and therefore the net amount of radiation from the surface is

only 230 W [10]. With every new layer added, the radiation loss will be reduced further. In Multi-layer Insulation, dozens of these layers are placed next to each other. It is imperative that the layers are in minimal thermal contact. This is achieved by placing coarse meshed silk or plastic net between them, reducing the amount of thermal bridges. Typical MLI blankets achieve effective emissivities in the range of 0.05 to 0.001, while the smallest values are only achievable under ideal circumstances (meaning no conduction between layers) [11].

2.4 Specific heat capacity

The specific heat capacity of a material $c_p(T)$ is defined as the amount of heat [J] needed to raise the temperature of 1 kg of the material by 1 K. Equivalently, the energy a given material with temperature T and mass m carries is

$$Q = c_p(T) \cdot m \cdot T. \quad (9)$$

There are two types of heat capacities for any given material. The mentioned c_p describes the specific heat capacity at constant pressure, while c_v is relevant in processes where the volume of the material fixed. As a general rule, the latter value is only significantly lower than c_p for gases.

Whenever the specific heat of a material is mentioned in the following, the value c_p is implied.

3 General assembly of PENeLOPE

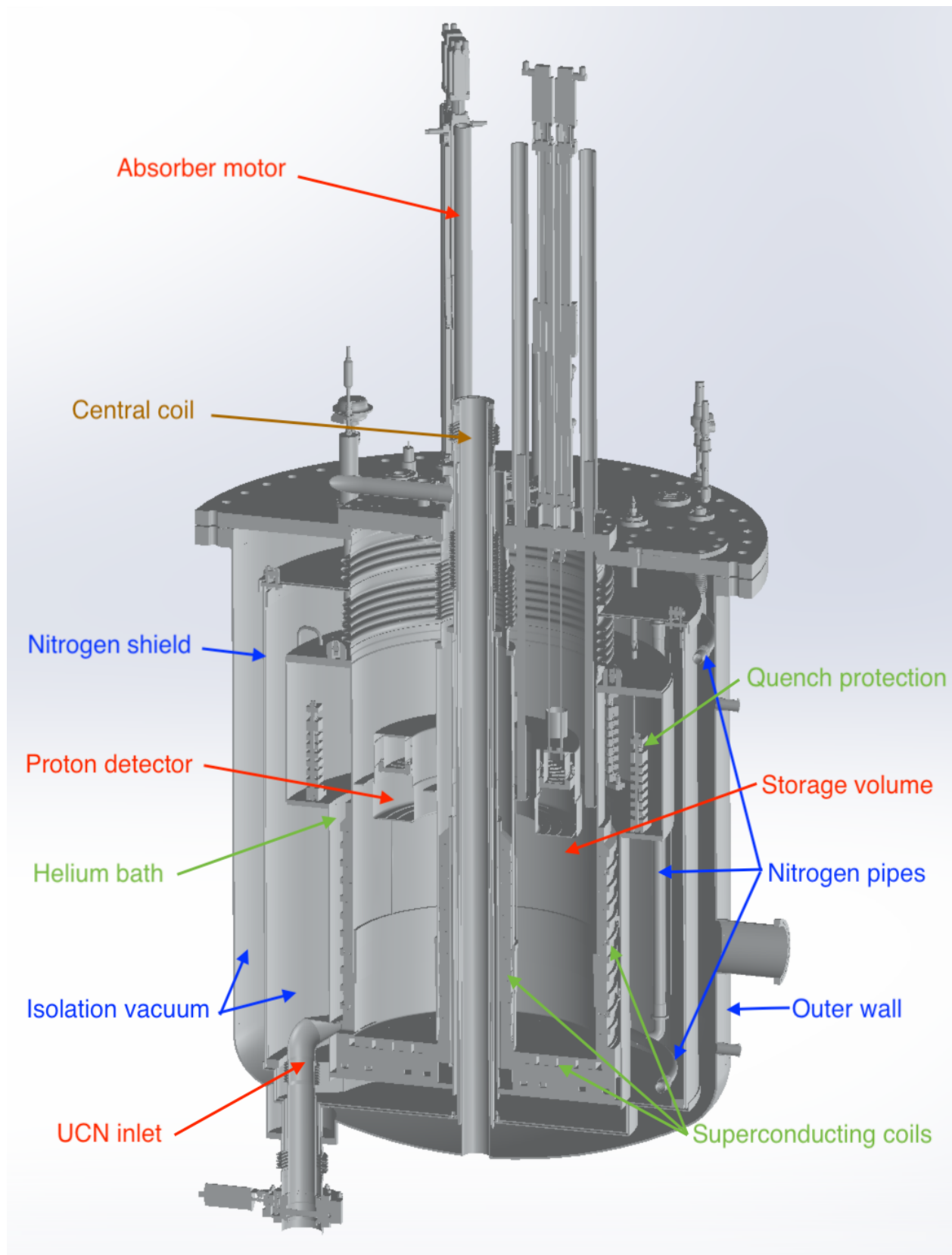


Fig. 4: Cross section of the PENeLOPE experiment. Note that neither the absorber motor nor the proton detector is built into the test assembly.

Figure 4 shows a cross section of the PENeLOPE experiment.



Fig. 5: Central MLI with temperature and Hall sensors fixed to it and the lid.

The detector is replaced by Multi-layer Insulation suspended from the lid (see figure 5).

In the following chapters, the assembly of PENeLOPE will be presented more in depth, which will be necessary for understanding the simulation. This will be done from the inside out, starting from the storage volume and ending in the outer wall of the assembly. For this purpose, a CAD model in the program Solidworks[®] is used.

3.1 The magneto-gravitational trap

The ultra-cold neutrons are trapped by magnetic multipole fields with large gradients. Neutrons interact with magnetic fields because of their magnetic moment $\mu_N = -60.3 \frac{\text{neV}}{T}$ arising from the electric charge of the quarks composing it [12].

Figure 6a shows the assembly of the superconducting NbTi magnets. The storage volume is surrounded from all sides except the top by 28 trapping coils. From coil to coil, the direction of the current alternates, creating a local minimum of the magnetic field inside the storage

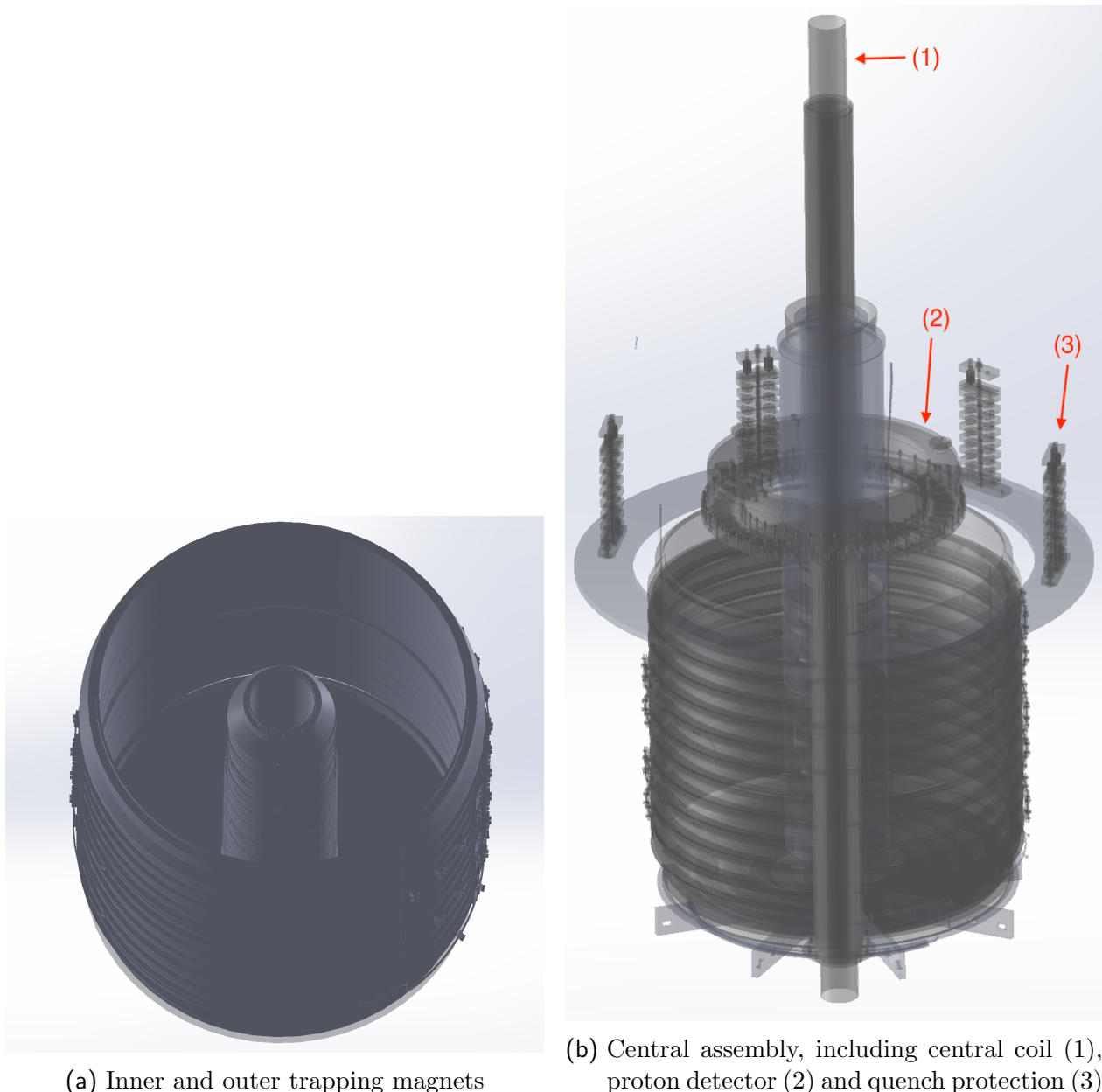


Fig. 6: Inner assembly of PENELOPE

volume. Neutrons with magnetic moments aligned opposite the field lines (low-field-seekers) are thereby trapped, since they do not have enough kinetic energy to escape the potential well. However, the fields from the solenoids cancel each other in some regions. This would allow for spin flip of the neutrons, turning low-field-seekers into high-field-seekers and thereby a loss of UCN. To fill the zero-field regions, a central coil is fitted inside the smaller ring of coils, creating an additional, azimuthal field.

Figure 6b shows this central coil as well as the proton detector and the quench protection. The latter is used to prevent overheating of the magnet in the case of a transition from the superconducting to a normal conducting phase ("quench").

Several measures have been taken to minimize heat flow from the central coil to the inner coils:

- Flow of cooling water through the coil
- Surrounding of the coil with an insulating Armaflex® mat
- Inclusion of the space between the inner wall and the helium container to the isolation vacuum (see section 3.4)
- Fitting of Multi-layer Insulation between the inner wall and helium container

The magnets consist of a stainless steel housing with ridges of about 4.6 cm width and 4.4 cm depth, where the coils are wrapped into. In the simulation, the housing and coils will be treated as one object, which has a total mass calculated to be 2586 kg (see appendix A).

3.2 The helium tank

Figure 7 shows the helium tank along with the lid and the connecting elements. Helium is filled through the inlet (blue), while the evaporated helium leaves the container through the outlet (green). As the assembly cools down, helium will start to condensate, so that the magnets and quench protections are eventually bathed in liquid.

The purple and red connections are used for temperature and liquid filling level measurements, while the yellow connection is used for the power supply of the magnets. The unhighlighted parts are the mountings for the helium container.

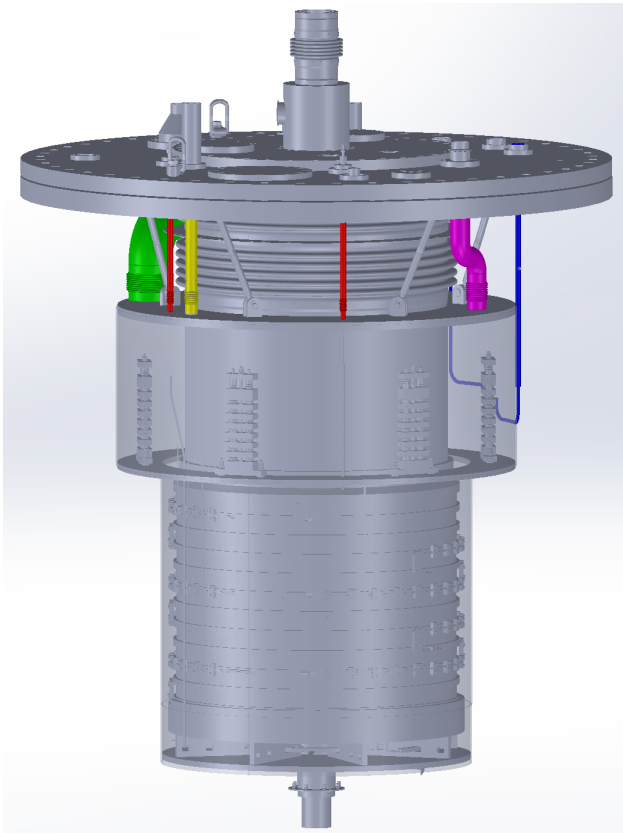
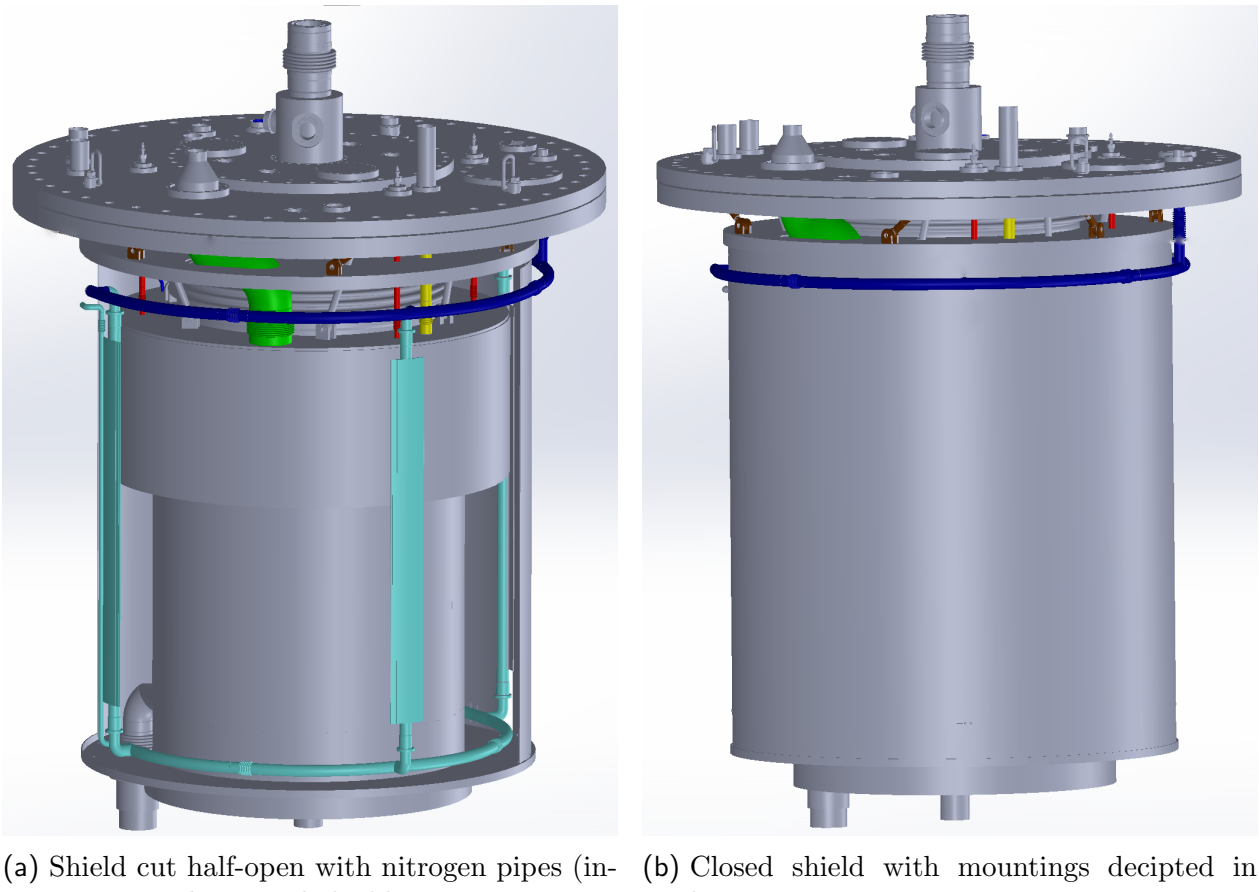


Fig. 7: Helium tank (transparent) with connections highlighted.

3.3 The nitrogen shield

This part of the assembly serves the purpose of minimizing the heat flow to the helium container with the goal of reducing the amount of helium needed for cooling (see figure 8). The shield and pipes are made of aluminum owing to the fact that this material has a high thermal conductivity, achieving a greater heat flux from the entire shield, through the pipes and into the liquid nitrogen running through them. These pipes are assembled in the following manner: Four pipes run along the shield and are in thermal contact with it, allowing for conductive heat transfer from the shield to the nitrogen. The thin pipe shown on the leftmost side in figure 8a is not connected to the shield. One circular pipe is placed between the helium tank and the shield, while another circular pipe runs between the shield and the outer wall. The shield covers the entire helium tank so that there is no direct radiation from the outer wall. This should greatly minimize the total heat flow to the central assembly, since the temperature gradient between the very cold helium tank and the cold shield is smaller than between the helium tank and the warm outer wall. Note that a smaller temperature



(a) Shield cut half-open with nitrogen pipes (inner pipes shown in light blue, outer pipes in dark blue).
 (b) Closed shield with mountings depicted in brown.

Fig. 8: Liquid nitrogen Shield

gradient is especially significant in the case of thermal radiation, as shown in eq. (6). In order to reduce the radiation to the shield, the outside of it is fully covered with a 30-layer MLI sheet.

3.4 The outer wall and lid

Figure 9 shows the entire assembly of PENeLOPE. The space between the outer wall and the shield is *not* hermetically isolated from the space between the shield and the helium container. This space is evacuated and will be called the isolation vacuum. The reason for creating a vacuum is that the convective heat transfer through air would be much greater than pure radiative heat transfer through vacuum (see appendix B for demonstration).

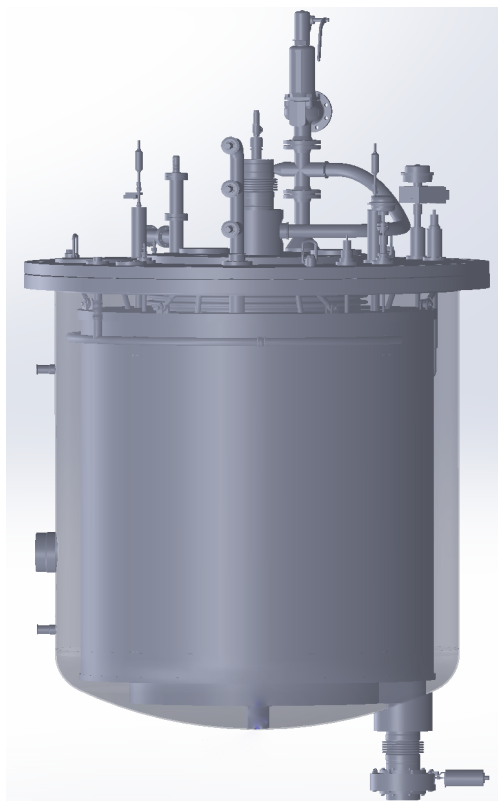


Fig. 9: Whole build, with outer wall transparent

4 Simulation with Simulink®

Simulink® is a graphically-oriented software tool for simulating mathematical models. It is a subprogram of MATLAB® and is based on its numerical solution algorithm. For the simulation, the add-on Simscape™ is used. This enables the creation of physical models within the Simulink® environment.

Simulink® provides various switching blocks, between which the data flow is realized by way of connecting lines. It is also possible to include custom MATLAB® functions in a simulation. Before explaining the simulation for the cooling cycle of PENELOPE, the used blocks will be presented.

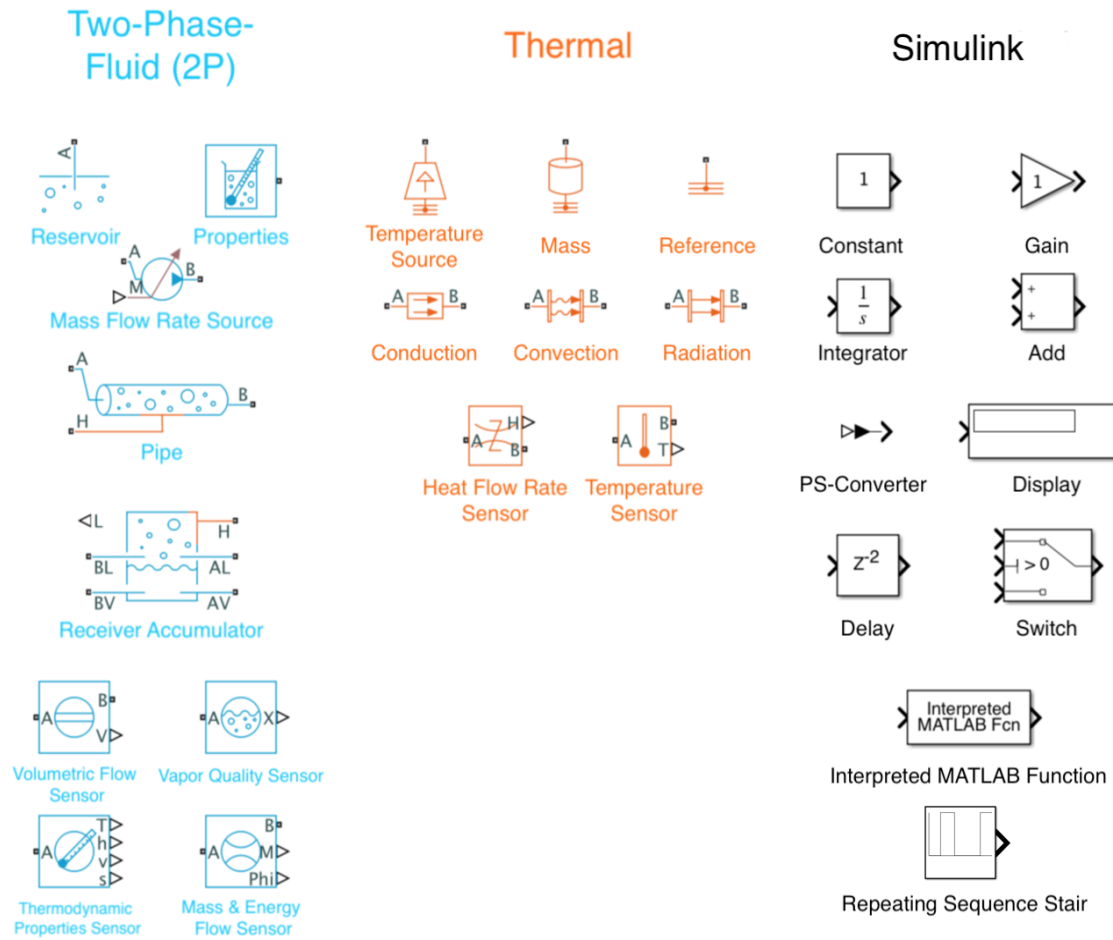


Fig. 10: Simulink® and Simscape™ blocks used for the simulation

4.1 Used blocks in the Simulink® simulation

With the Two-Phase-Fluid library in Simscape™, it is possible to model systems with a substance that is part liquid and part gas. In the following, the term "fluid" can mean either liquid or gas. The Thermal blocks model fundamental thermal effects, while the Simulink blocks function as purely mathematical operators.

Figure 10 shows all blocks that appear in the simulation. Each will be explained briefly.

- **Reservoir:** Sets the boundary conditions in a two-phase fluid network; has a set pressure and temperature

- **Properties:** Provides properties of the fluid
- **Mass Flow Rate Source:** Represents an ideal energy source that can maintain a controlled mass flow rate
- **Pipe:** Models pipe flow dynamics due to viscous friction losses and convective heat transfer with the pipe wall
- **Receiver Accumulator:** Models a container of fluid and the convective heat transfer between the walls and fluid
- **Volumetric Flow Sensor:** Measures volumetric flow
- **Vapor Quality Sensor:** Measures vapor fraction
- **Thermodynamic Properties Sensor:** Measures temperature, specific enthalpy, specific volume and specific entropy
- **Mass & Energy Flow Sensor:** Measures mass and energy flow rate
- **Temperature Source:** Ideal energy source that can maintain a constant absolute temperature
- **Mass:** Models an internal energy storage according to eq. (9)
- **Reference:** Represents a reference point where the temperature is equal to absolute zero
- **Conduction:** Models heat transfer by conduction through a layer of material according to eq. (1)
- **Convection:** Models heat transfer by convection due to fluid motion according to eq. (2)
- **Radiation:** Models heat transfer by radiation between two surfaces according to eq. (6)
- **Heat Flow Rate Sensor:** Measures the heat flow rate through the block
- **Temperature Sensor:** Measures the temperature difference between ports A and B
- **Constant:** Outputs the specified value
- **Gain:** Multiplies the input by the specific value

- Integrator: Carries out continuous-time integration of the input signal
- Add: Adds inputs
- PS-Converter: Converts the physical input signal to a Simulink/Mathematical output signal or vice-versa
- Display: Displays the input value
- Delay: Delays the input signal by specified number of samples
- Switch: Outputs input 1 when input 2 satisfies criterion; otherwise, outputs input 3
- Interpreted MATLAB Function: Passes the input value to a MATLAB function, which returns a single value that is then the output of the block
- Repeating Sequence Stair: Outputs specified values depending on time.

The legend of the subsystems in the simulations is the following:

- **Brown**: Exterior parts
- **Magenta**: MLI
- Light gray: Nitrogen shield
- Dark gray: Helium container components
- **Turquoise**: Nitrogen cycle
- **Blue**: Helium cycle
- **Purple**: Magnets
- **Yellow**: Heat flow sensors

4.2 Remarks on the simulation and overview

Initially, the simulation was split up into two separate ones. The reason for that is the following: If there is helium cycle included in the simulation, other parts of it need to be built differently because of characteristics of the Receiver Accumulator: This block represents an infinitely thin surface on the interior of helium container and around the magnets, which determines the interaction with them and the fluid. The surfaces of the involved components facing the helium need to be connected on the same thermal line towards the Receiver Accumulator, giving them the same surface temperature in the simulation.

If there is no helium involved (air-filled container), the simulation should include convective heat transfer blocks to represent the interactions in the interior of the container. This was done and is shown in appendix C.

To not exceed the length of this thesis, only the more general simulation involving helium will be thoroughly explained in the main part. The consequences of this regarding the results are negligible, as is shown in appendix D.

Note that, in the simulation that will be explained in the following, it is still possible to turn off the helium flow and therefore examine and compare the results to the measurements of the cooling using only liquid nitrogen.

The relevant dimensions of each element as well as the used material constants as used in the simulation are presented in appendix E.

Figures 11 and 12 together show the simulation of the heat flow in PENeLOPE.

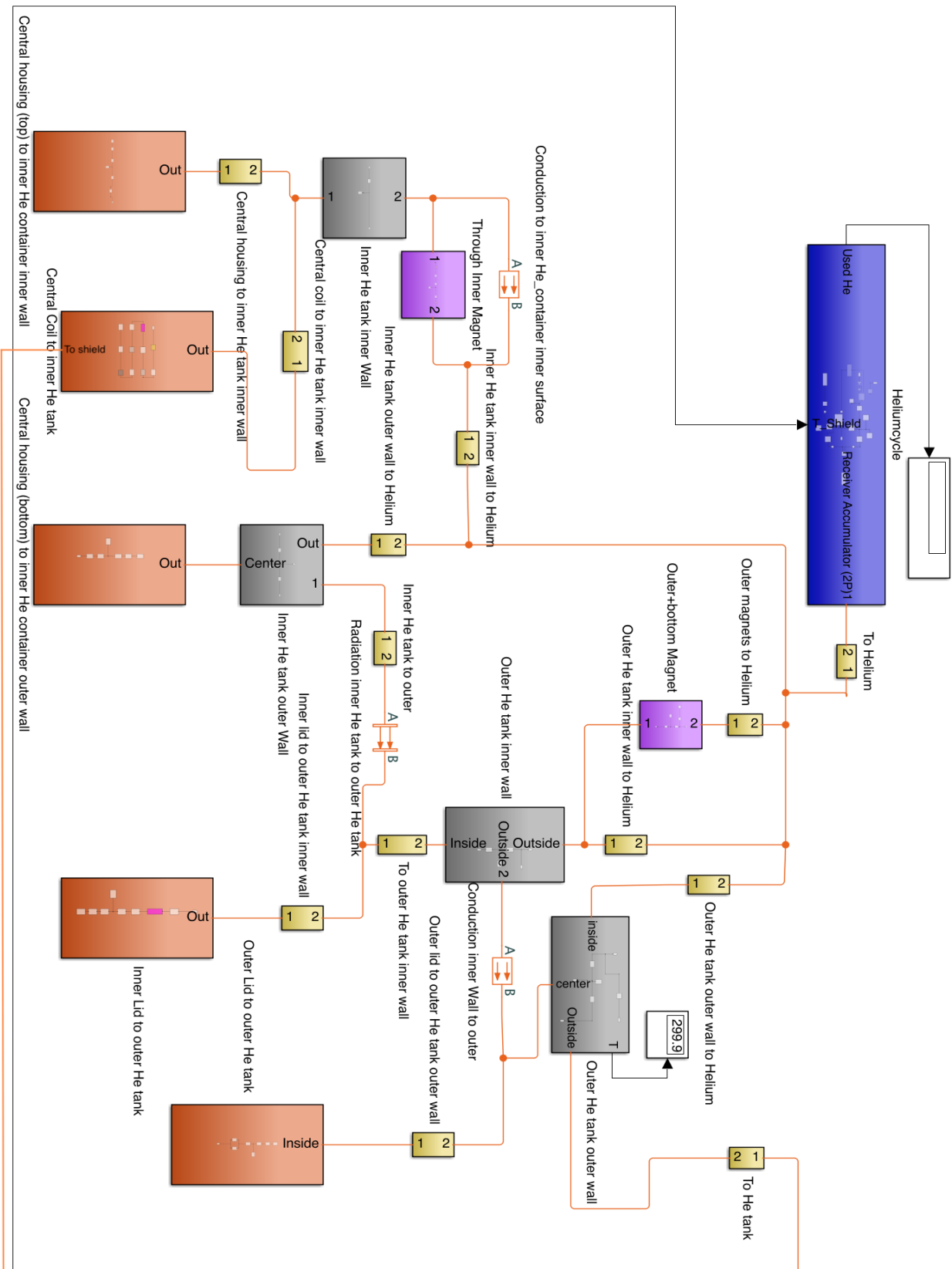


Fig. 11: Thermal simulation involving the helium container

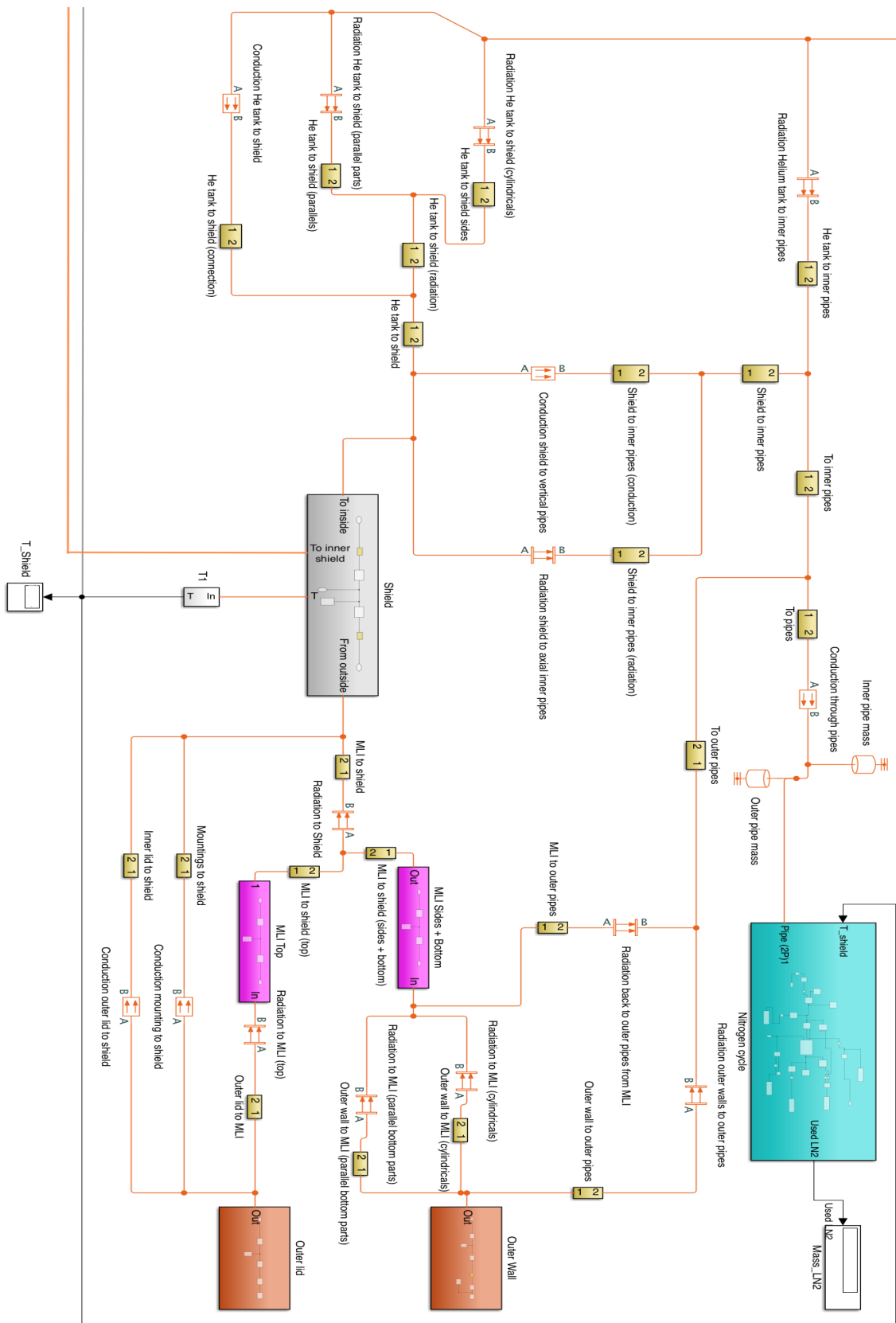


Fig. 12: Thermal simulation up to and including the nitrogen shield. Note that the lines leaving the image on the top connect to the lines leaving fig. 11 on the bottom.

4.3 Simulation involving the nitrogen shield

Figure 12 shows all parts of the simulation that involve the nitrogen shield and its interactions with the exterior parts, helium tank, as well as the nitrogen itself. This part of the simulation will now be explained in detail.

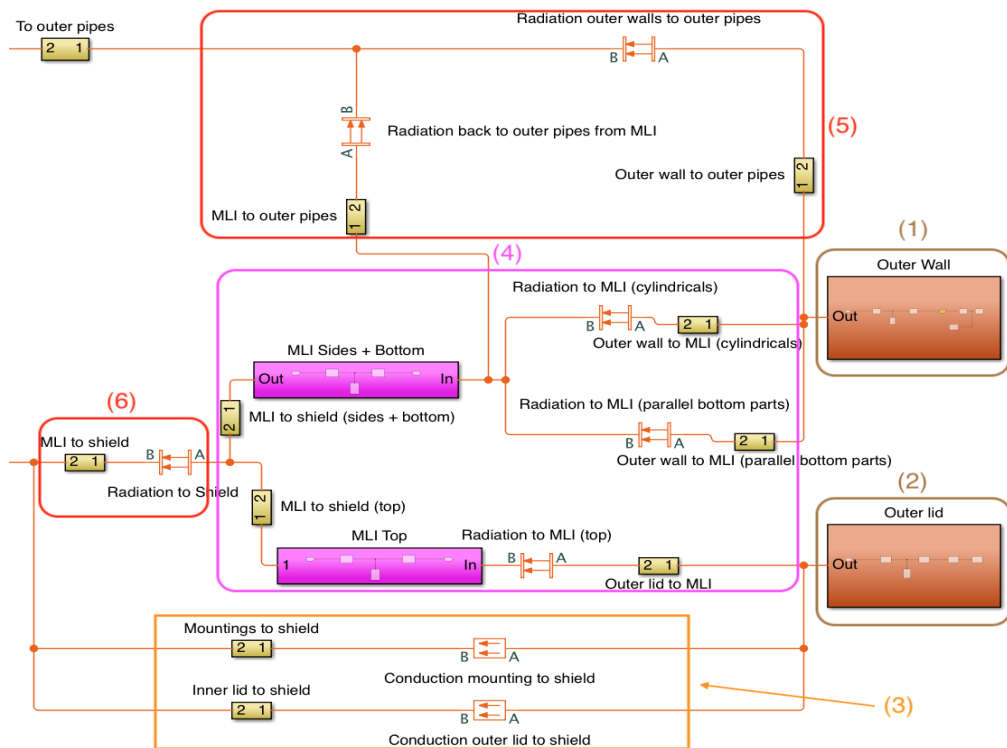


Fig. 13: Thermal simulation from the exterior to the shield and outer pipes

Figure 13 depicts the part of the simulation that resembles the heat flow from the exterior to the shield and outer pipes.

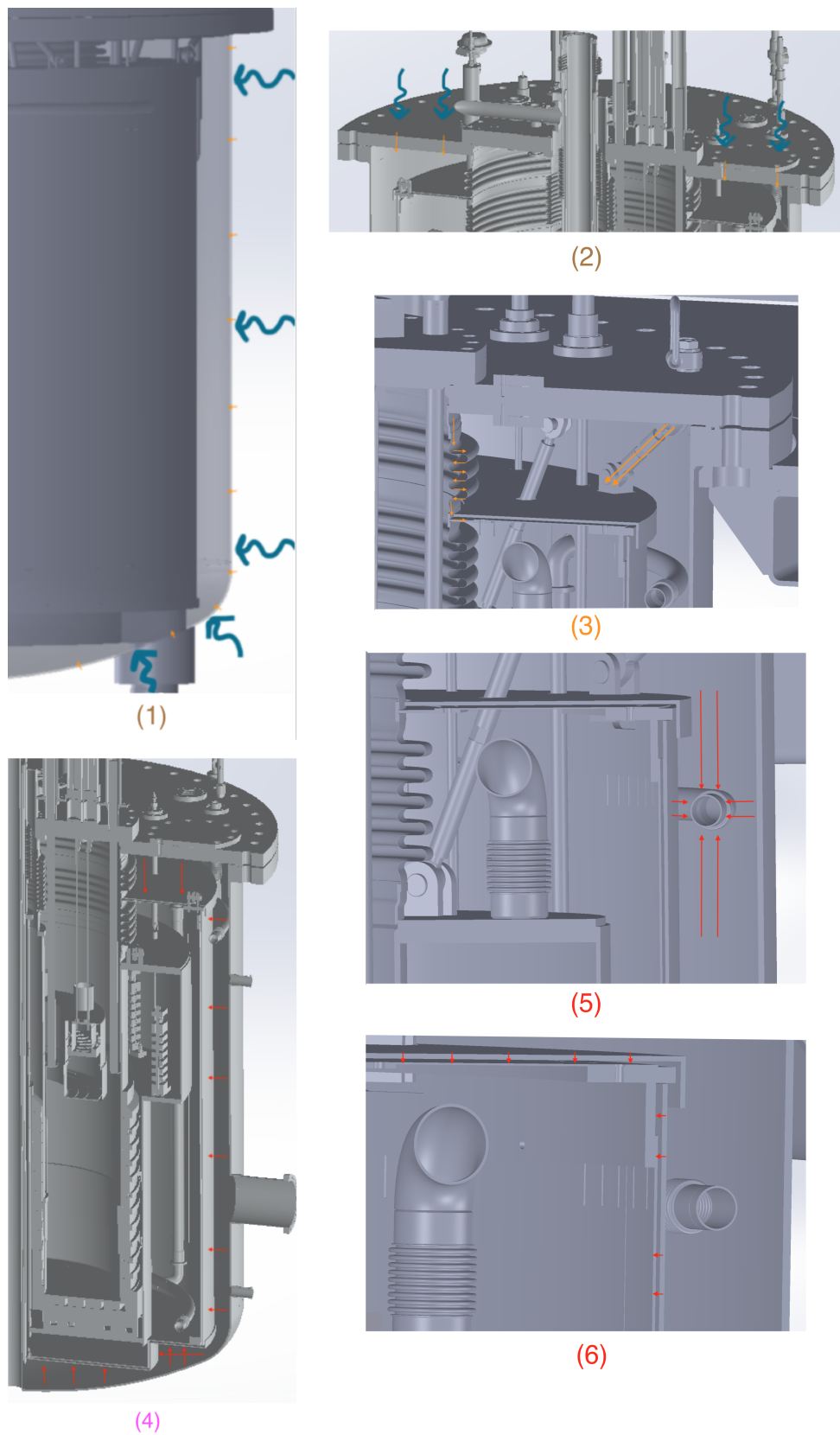


Fig. 14: Heat flow from the exterior to the shield and outer pipes

Figure 14 shows the thermal processes that this part of the simulation stand for. Segments (1) and (2) represent the convection to the outer wall and lid as well as the conduction to their interior surfaces. Segment (3) of the simulation represents the direct conduction from the outer lid to the shield. The top part of the UCN container is corrugated, increasing the path d for heat to travel and therefore decreasing the total heat flow according to eq. (1). Apart from the direct thermal conduction from the outer parts to the shield, they give off thermal radiation through the isolation vacuum to the MLI covering the shield. This process is represented in segment (4). The outer wall and the MLI also radiate to the outer nitrogen pipes (5). Segment (6) simulates the radiation from the MLI to the shield. For the radiation coefficient between the cylindrical parts of the MLI and outer wall, eq. (8) is used, while that between the parallel parts is calculated with eq. (7). The area of the nitrogen pipes is assumed to be parallel to the other involved surfaces.

Notice that - for simplification reasons - the outer lid is treated as separate from the inner lid and that the UCN inserter is not considered.

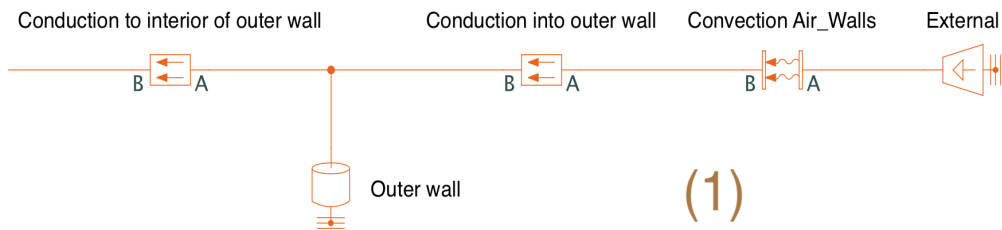


Fig. 15: Simulation of the heat flow from exterior to the interior of the outer wall

To get an insight into how the heat flow from the exterior, to the outer surface, and through the material is simulated, see figure 15. The constant temperature source on the right is set to $292.15\text{ K} = 20\text{ }^{\circ}\text{C}$. The next block represents the convection of the air with said temperature to the outer walls. The three blocks from then on represent the conduction **into** the outer wall, towards the thermal mass assumed to be centered in the middle and finally the conduction to the inner surface of the outer wall.

This is the way the conduction through all components is simulated.

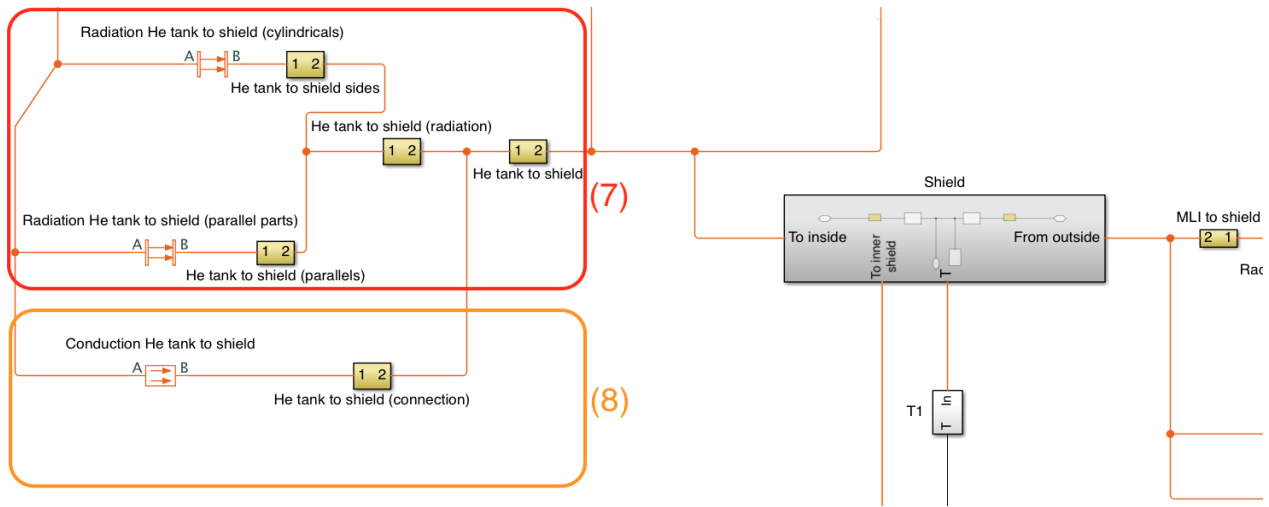


Fig. 16: Simulation of the heat flow between the helium tank and the shield

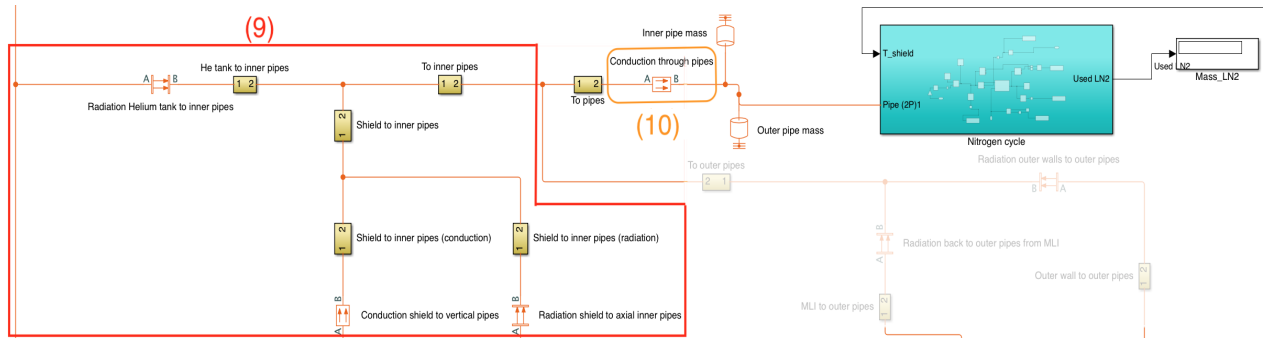
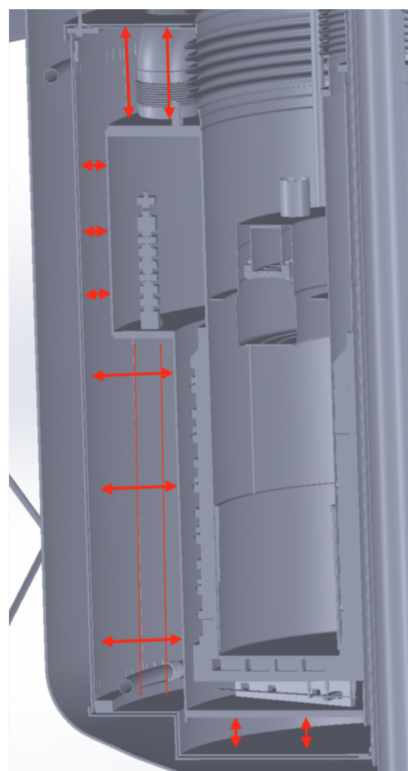
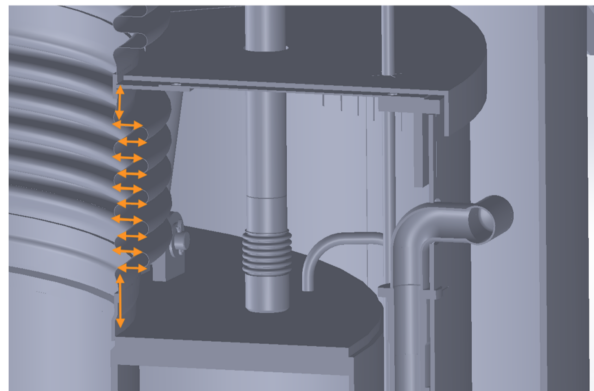


Fig. 17: Simulation of the heat flow to the inner nitrogen pipes from the shield and helium tank

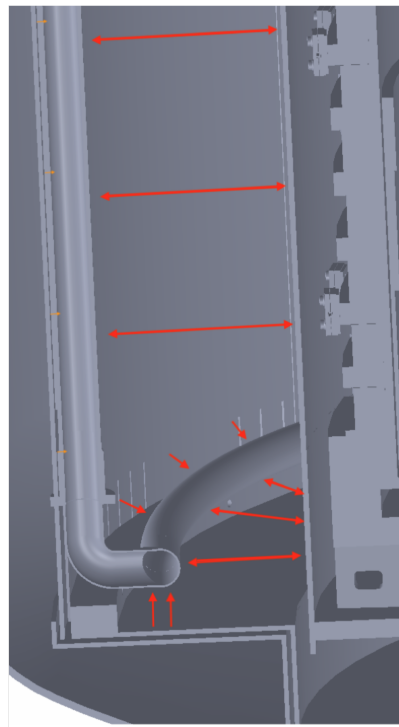
Figure 16 shows the part of the simulation that simulates the heat flow from the helium tank to the shield or vice-versa. The remaining elements of the part of the simulation that involve the nitrogen shield are shown in figure 17.



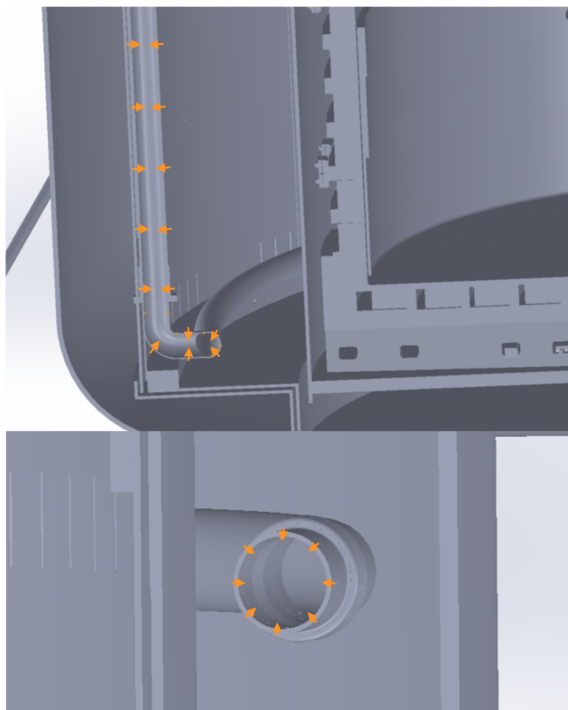
(7)



(8)



(9)



(10)

Fig. 18: Heat flow from the helium tank to shield or vice-versa, as well as to the inner nitrogen pipes

Figure 18 shows the processes simulated in figures 16 and 17. Segment (7) stands for the radiation to/from the helium tank, while segment (8) represents the conduction through the top of the UCN container to/from the helium tank. Since the helium tank can be colder or hotter than the shield depending on if helium is involved or not, the arrows point in both directions. Segment (9) represents the radiation from the shield and helium tank to the nitrogen pipes, while segment (10) simulates the conduction from the inner and outer pipe surfaces to the nitrogen itself.

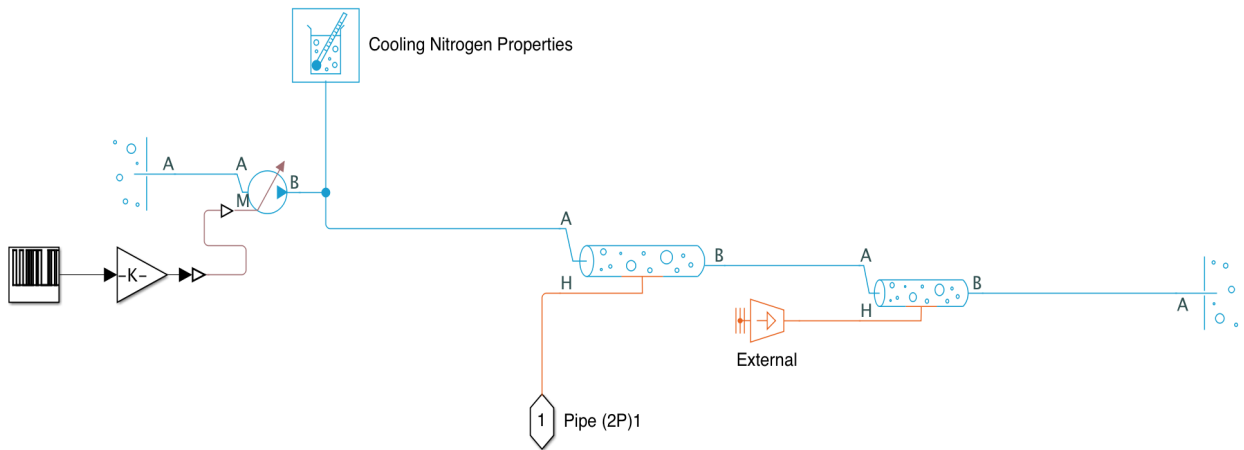


Fig. 19: The nitrogen cycle

Lastly, the nitrogen cycle will be explained (see figure 19). The left reservoir, which is set to 77 K, represents the liquid nitrogen dewars, while the right reservoir stands for the tank where the used nitrogen ends up. The pipes are represented by the 2-phase-fluid pipe in the center. The pipe on the right side represents a heater (set to 50 °C), which is also present in the actual experiment. In the simulation, the nitrogen flow is powered by a mass flow rate source. The input is determined by the repeating sequence stair, allowing us to simulate a non-continuous nitrogen flow¹.

A mass flow sensor was installed in the laboratory, but it turned out to be defective. Since it took ≈ 10 hours to empty a 100 l dewar, a mass flow of $2.25 \frac{\text{g}}{\text{s}}$ can be estimated. However, this value is far from constant, since it depends on the applied pressure, which was regularly varied using compressed air.

During the testing of the simulation, an interesting observation was made: Without including the warm bath in simulation, oscillations were observed when the shield reaches temperatures

¹ The originally planned connection to a large nitrogen tank turned out not to be possible. This would have allowed for a continuous flow. Instead, individual dewars were used, which emptied regularly.

around 110 K and below (see figure 20). The reason for that are tiny amounts of unvaporized nitrogen leaving the system. As you can see, the net liquid fraction of the used nitrogen increases with the decreasing shield temperature (notice downward slope in the oscillations in figure 20). These oscillations leads to a great increase in computanional effort and therefore simulation time.

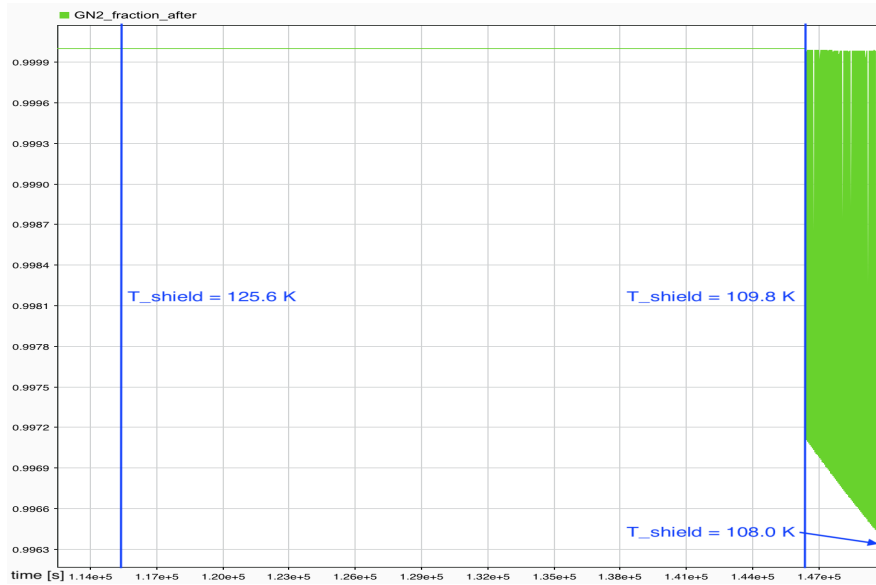


Fig. 20: Vapor fraction of the used nitrogen without the warm bath.

4.4 Simulation of the heat flow in and to the helium tank

In this part of the simulation, the helium tank is split into four segments (see figure 21). This allows for a more accurate representation of the heat flow at the cost of simplicity (for similar reasons, the magnet was split up into the inner part and the outer+bottom part). Notice that the upper part of the inner helium container is not included as part of the helium tank in the simulation. Since liquid helium will not reach this part of the tank (it is merely supposed to cover the quench protection), it will have a higher temperature than the rest. If it were to be included as part of the container, the measured temperature in the simulation would be (even) higher than the temperature that the sensors measure in the actual experiment, since they are located lower in the build (Simulink® treats a thermal mass as a mass point). Therefore, excluding the part from the simulation allows for a better comparison to the measurements.

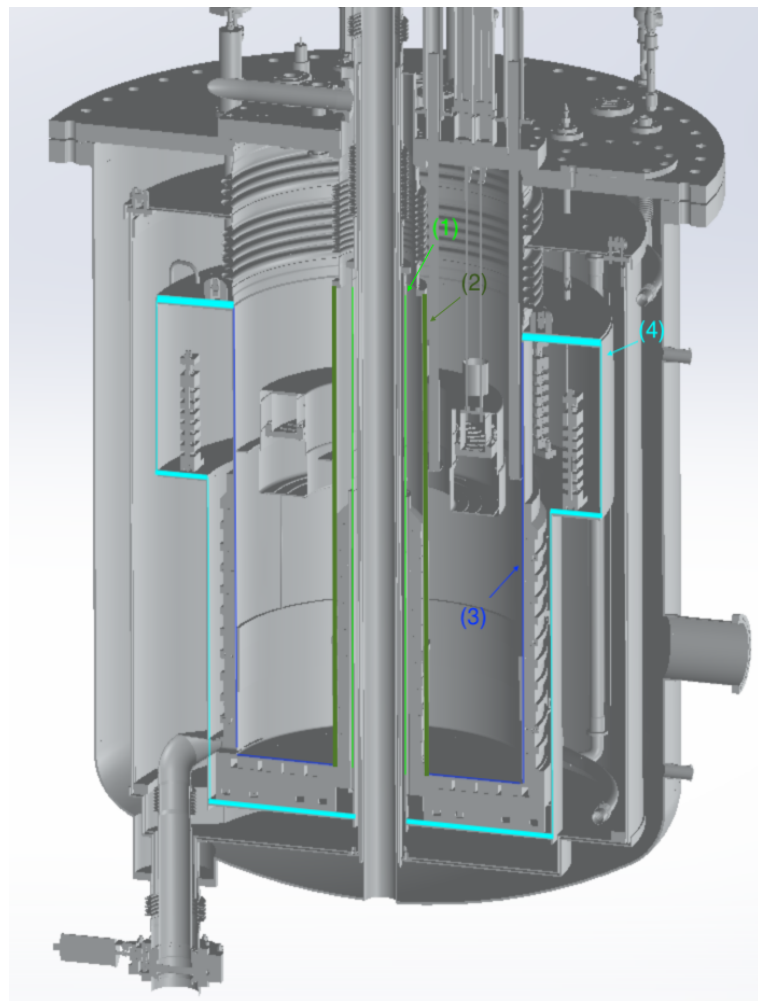


Fig. 21: Division of the helium tank: (1): Inner helium tank inner wall, (2): Inner helium tank outer wall, (3): Outer helium tank inner wall, (4): Outer helium tank outer wall

In theory, this segmentation of parts of components could be done for all elements of PENELOPE, making the simulation arbitrarily complex. However, since the heat flow to the helium tank is considerably different depending on the segment, it became evident that treating the entire component as the same thermal mass causes a distinct distortion to the results in contrast to other elements.

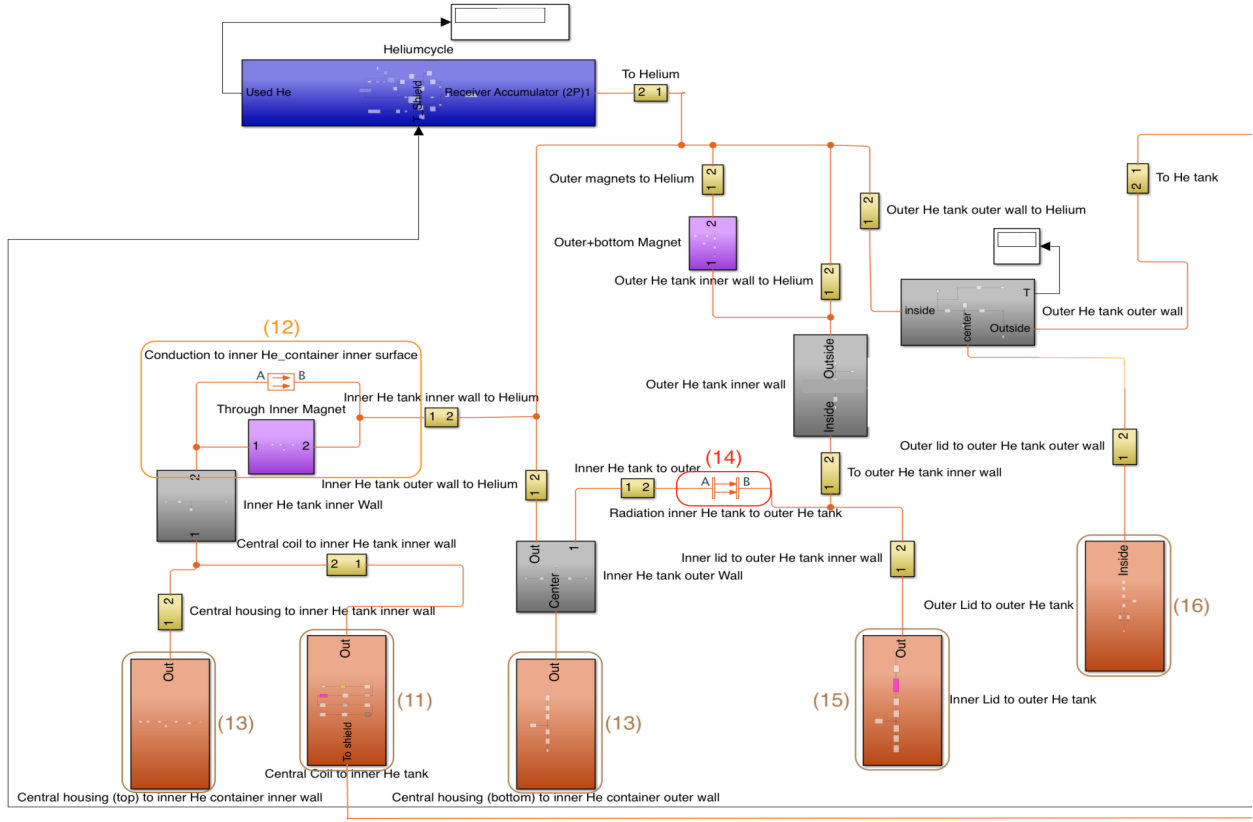


Fig. 22: Thermal simulation involving the helium container

In this section, the simulation of the heat flow involving the helium tank and the magnets will be explained (see figure 22).

Figure 23 shows sketches of the methods of heat transfer to the helium container and magnets.

Segment (11) simulates the heat transfer from the central coil to the inner helium tank. Heat flows from the central coil, through the insulating Armaflex mat and the outer wall. The outer wall then radiates heat onto the shield - MLI - shield assembly (mounted in the isolation vacuum) and then to the inner helium container. The inner shield is separated from the outer shield in the simulation, because otherwise the outer shield temperature in the simulation would be too high. However, since it is part of the outer shield in the actual assembly, the simulation needed to account for that: The line connecting to this subsystem from the bottom also connects to the outer shield (see fig.12). A conductive heat transfer block simulating heat flow from the inner shield to the outer shield is added to this connection.

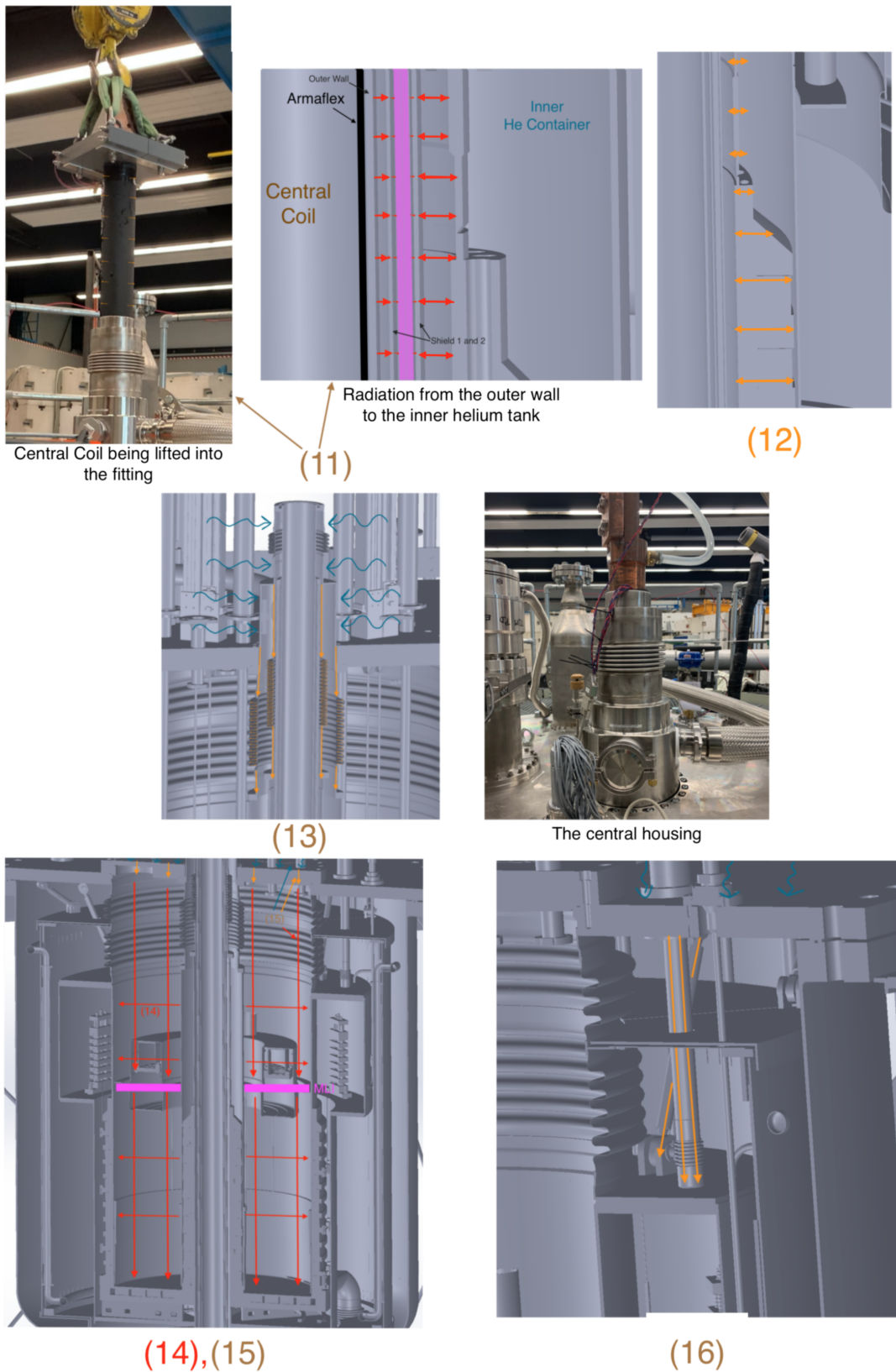


Fig. 23: Thermal processes involving the helium container

The elements inside (12) stand for the conduction through the inner helium tank inner wall and the inner magnet. The remaining sources of heat to the inner helium container come from the central housing on top of the assembly (13). The inner helium tank as well as the inner lid radiate heat towards the outer helium tank, which is represented by blocks (14) and (15). The external heat transfer to the outer helium tank outer wall through the connections is simulated by subsystem (16).



Fig. 24: Convection to helium from the magnets and helium tank

The lines leading to the helium cycle symbolize the convective heat transfer between the helium and the helium tank and magnets (see figure 24).

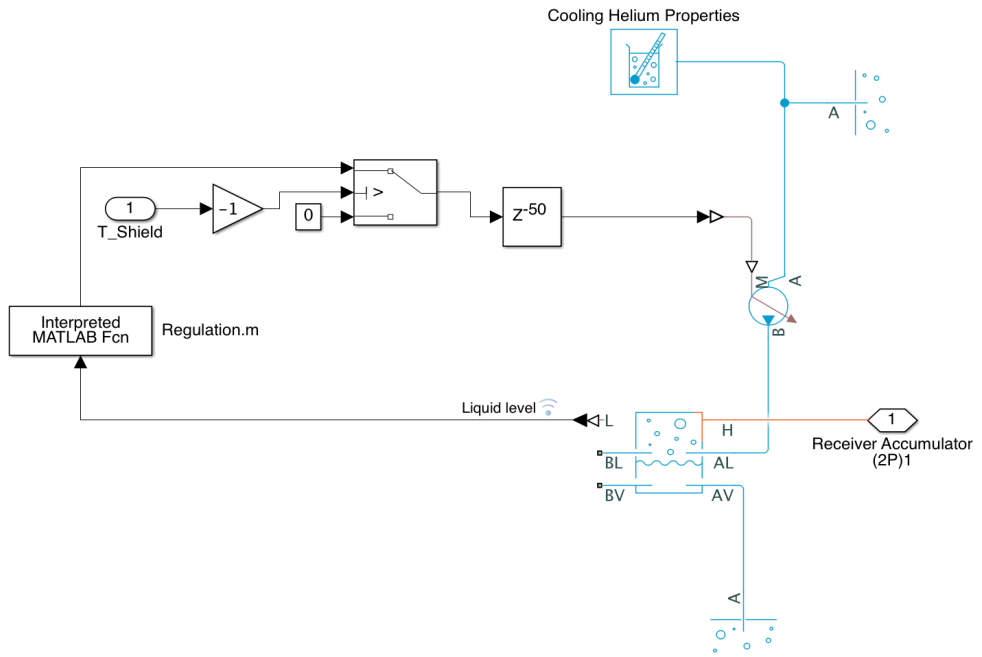


Fig. 25: The helium cycle

```

function regulate = regulation(liquidfr)
    if liquidfr >= 0 && liquidfr < 0.790
        regulate = 0.02
    else
        regulate = 0;
    end

```

Fig. 26: The regulation function

Lastly, let us look into the helium cycle (see figure 25). Liquid helium flows from the upper Reservoir (set to 4 K) into the Receiver Accumulator, where it evaporates and reaches the bottom Reservoir (set to 293 K). Similar to the nitrogen, the helium flow is powered by a mass flow rate source. The flow is regulated depending on the liquid level in the container, as well as the temperature of the shield. This allows us to turn on the helium flow only when liquid nitrogen has cooled down other components to the specified temperature in the switch. The Interpreted Matlab Function block passes the input (liquid level) to the function regulation.m (see figure 26), which turns on the helium flow only when the quench protection is not covered with liquid helium (see appendix F for the calculation of the necessary liquid level). The delay block serves the purpose of eliminating errors created by the algebraic loop

in the system.

5 Simulation results, comparison to measurements & discussion

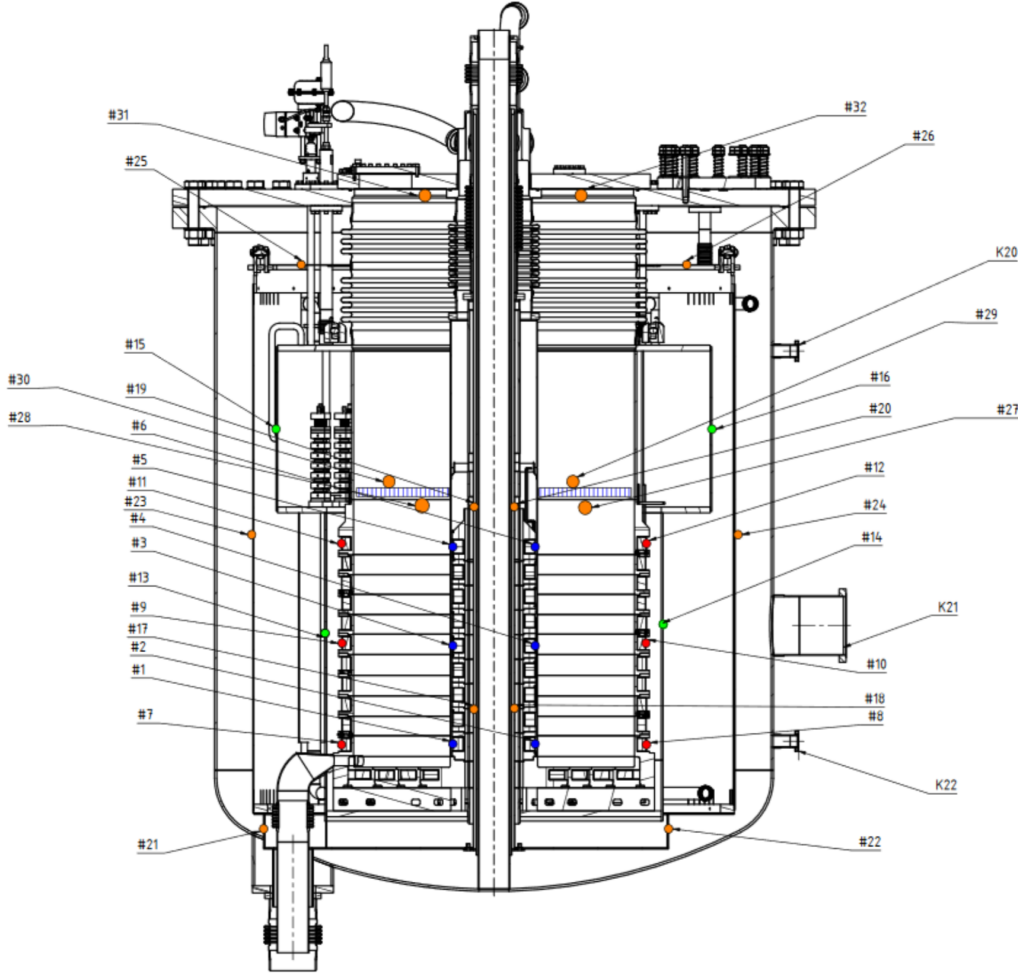


Fig. 27: The temperature sensor positions

Figure 27 shows the positions of the sensors in the cross-section of PENeLOPE. For a description on the positions and types of sensors that were used, see appendix G.

In the next section, the results of the simulation using only nitrogen will be presented and compared to the measurements. After that, the effects of helium in the simulation will be displayed. As mentioned, it was not yet possible to do measurements with liquid helium, so these results will be displayed without comparison. However, some plausibility checks will be done.

5.1 Results without helium

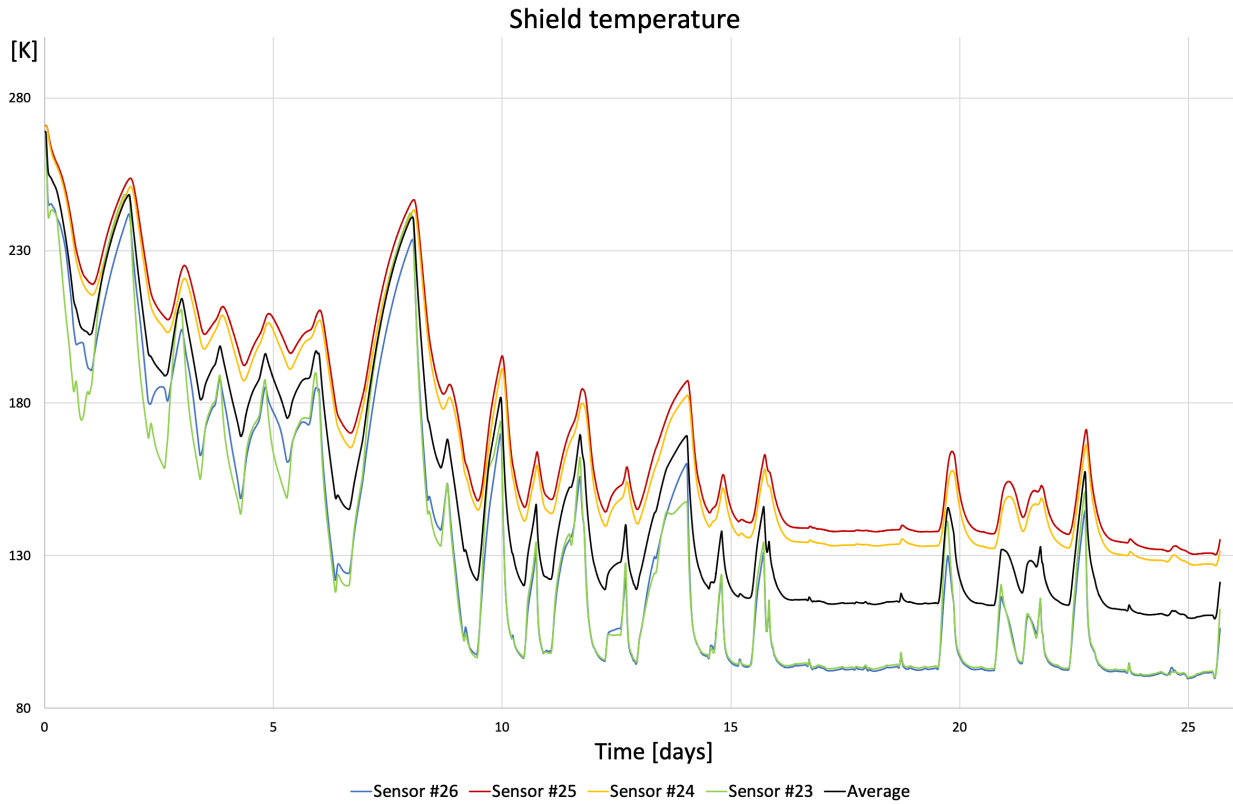


Fig. 28: Shield temperature over 26 days, including average

Figure 28 shows the measurements of the temperature sensors connected to the shield. The periods during which the dewar was empty and was not replaced right away are the reason for the periodical temperature increase.

In the actual experiment involving UCN, it is expected that a source of constant nitrogen flow is available. Therefore, it is of interest to know how long it would take for the shield to reach minimal temperature in this case. This will be done in the next section.

After that, the simulation results will be directly compared to other measurements.

5.1.1 Determining the cooling time for a continuous nitrogen flow

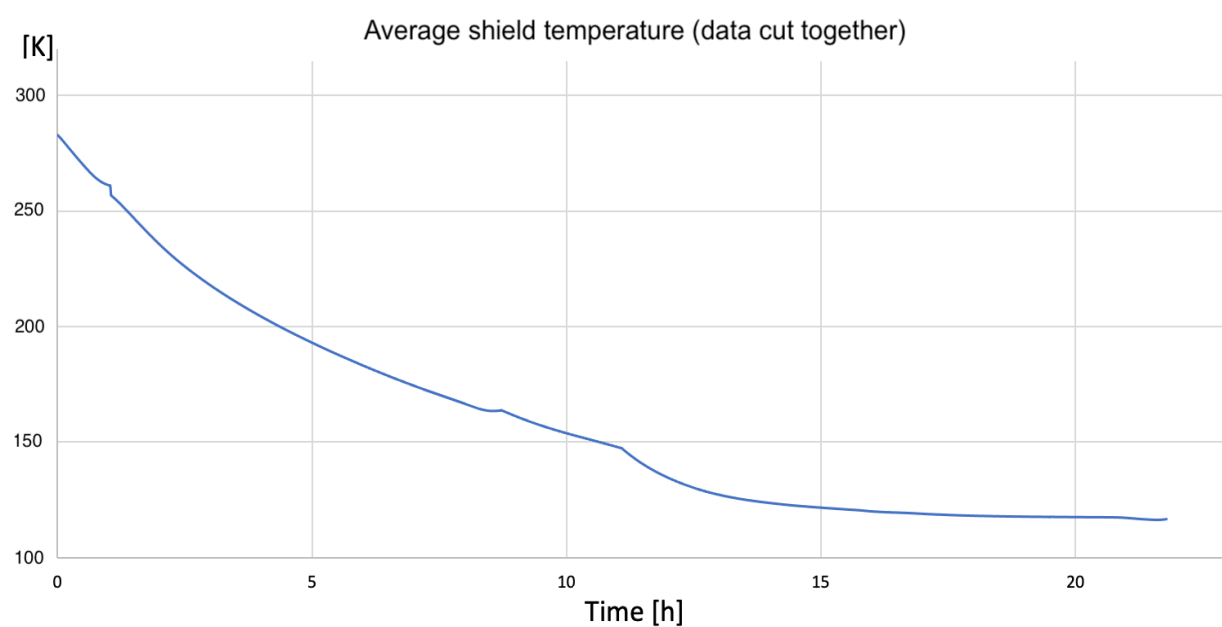


Fig. 29: Average shield temperature over 22 hours (using combined data)

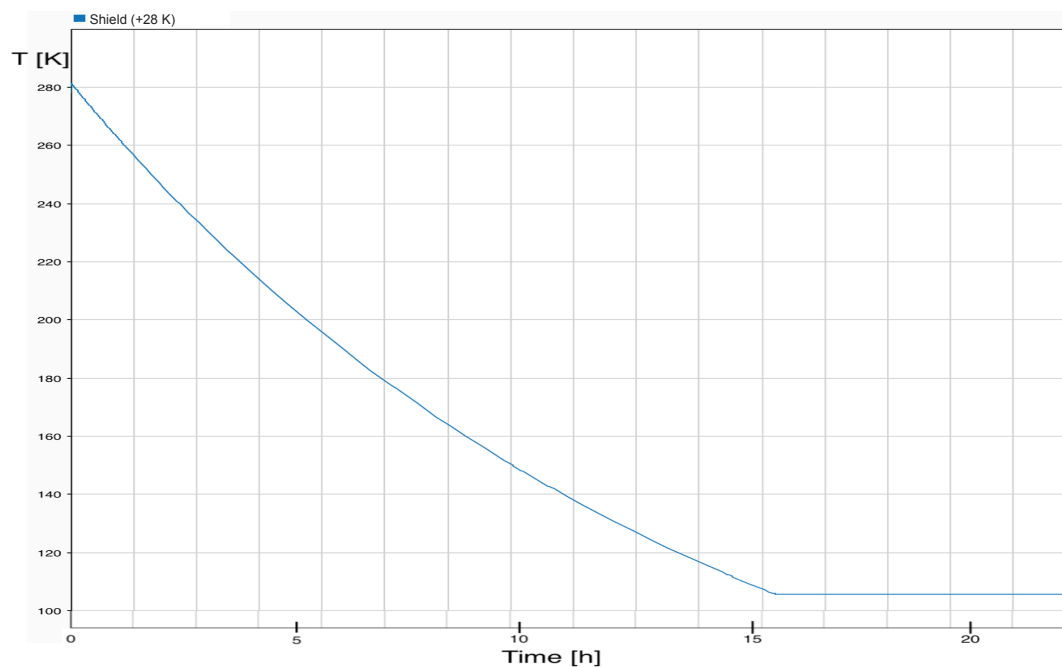


Fig. 30: Shield temperature over 22 hours in the simulation (initial temperature: 280 K)

To gain a clearer comparison to the simulation, a graph connecting the average shield temperature at periods with non-zero nitrogen flow is made (see figure 29). As you can see, the temperature measurements do not start at the first instance of cooling. This will be accounted for by an adjusted initial shield temperature in the simulation (280 K). Comparing the data to the shield temperature in the simulation using a constant nitrogen flow of 2.25 g/s \equiv 10l/h, we observe good qualitative agreement (see figure 30).

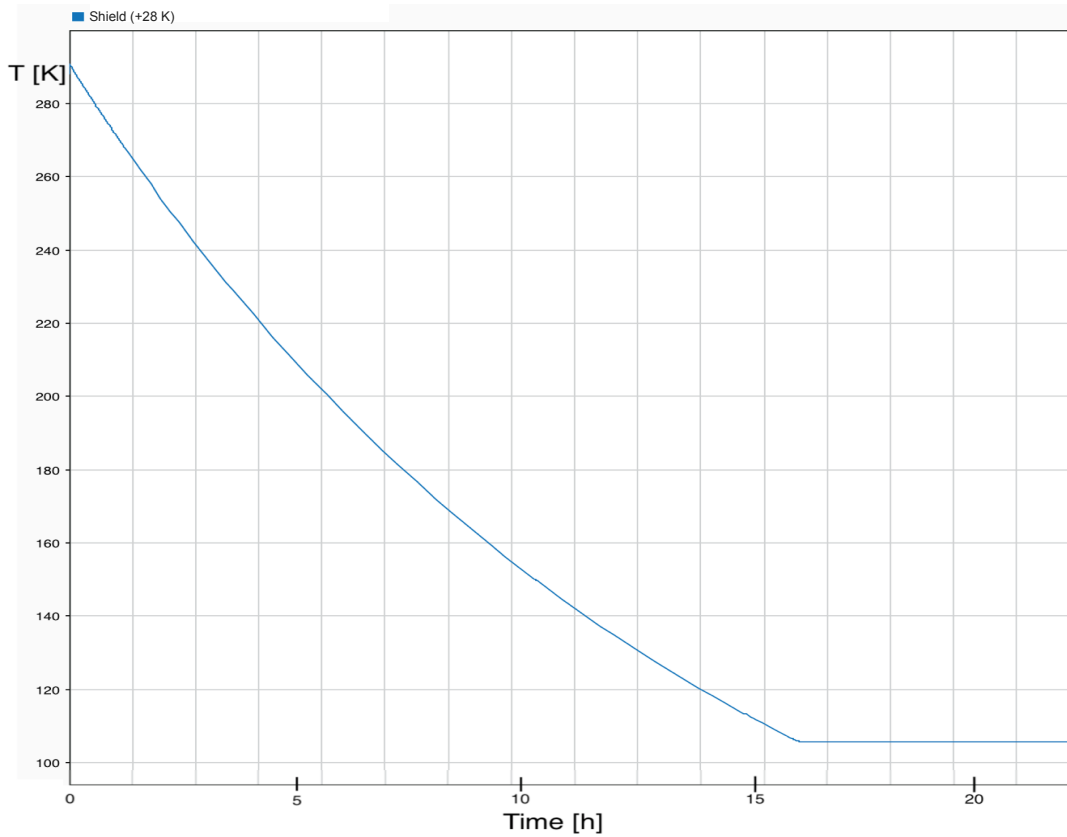


Fig. 31: Shield temperature over 22 hours in the simulation (initial temperature: 293 K)

With this information, we can now start from an initial shield temperature of 20°C. From this, we can extrapolate the actual cooling time needed to reach equilibrium from start to finish. The resulting graph is shown in figure 31. As you can see, a constant flow of 10l/h would be sufficient to cool down the shield to minimal temperature within approximately 16 hours.

5.1.2 Comparison of simulation results and measurements

For the following measurements, it is not reasonable to cut data with non-zero nitrogen flow together, because the regarded temperatures are not as directly linked to the nitrogen flow as the shield itself. Therefore, a different method is chosen: Instead of cutting the **data** together to represent a constant nitrogen flow, the flow in the **simulation is modified** to mirror the raw measurements. The Repeating Sequence Stair block is used to resemble the nitrogen flow over the first 10 days of measurement. This is done by determining the periods at which nitrogen was and was not connected and translating this into the block parameters.

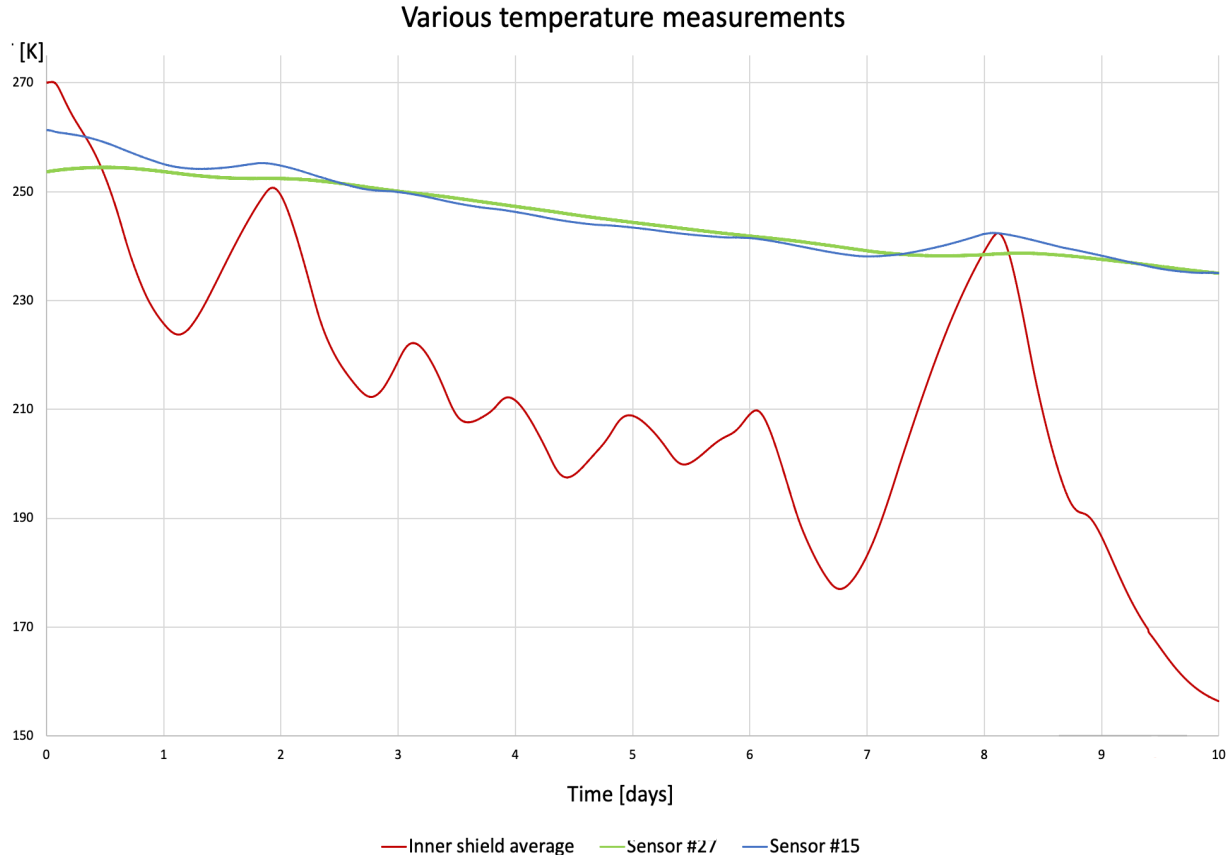


Fig. 32: Temperature measurements of various sensors.

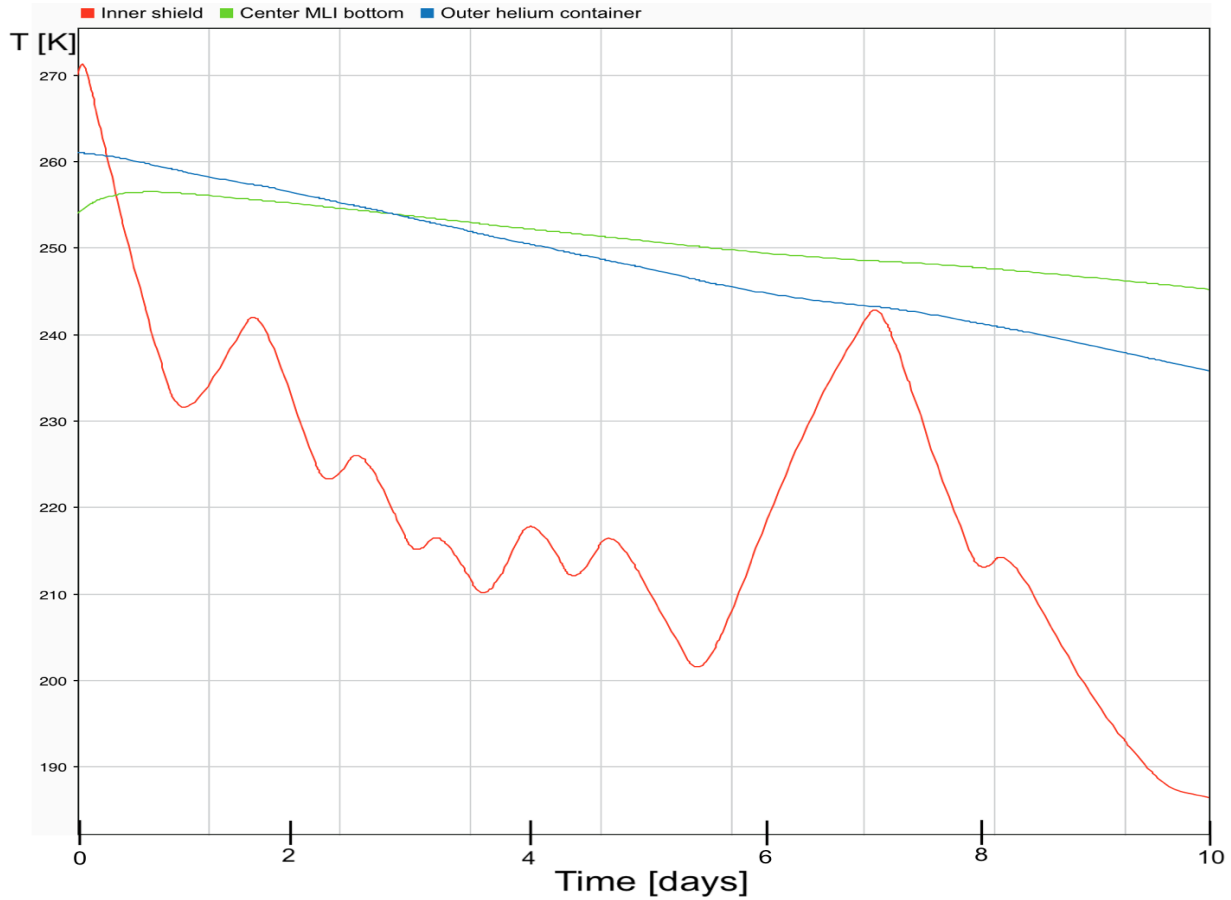


Fig. 33: Simulation results of the same components as the sensors of figure 32.

Figure 32 shows the measurements of sensors #15 , #27 and the average of sensors #17 - #20 (inner shield) over the first ten hours. Figure 33 shows the simulation results for the same parts of the assembly.

Qualitatively, the results properly mirror the measurement. Quantitatively, discrepancies can be observed (see tabular 1).

The main source of these disparities is that the simulation assumes a constant nitrogen flow (if on). In the experiment, the flow fluctuates significantly due to frequent variation of the applied pressure, which was not documented. Additionally - even in the case of a constant nitrogen flow - the observed emptying time of each dewar cannot be directly translated into a nitrogen flow in the simulation: As a result of heat flow to the dewar itself, as well as to the ~ 2 meter connection to the assembly, additional nitrogen evaporation would need to be accounted for.

Some added distortion to the simulation results could be a result of the fact that the actual

material constants are strongly temperature dependend, which could not be accounted for. This is a great simplification, but it is without alternative: Simulink® does not have a feature for temperature- or time-dependent block parameters.

Tab. 1: Quantitative comparison of simulation results and measurements

Part	Maximal discrepancy of simulation and measurement
Inner shield average	34 K
Center MLI bottom	10 K
Outer helium container	4 K

5.2 Results with helium

To gain a full picture of the cooling cycle of PENELOPE, the simulaiton results of the process involving the direct cooling of the magnets with helium will be regarded. Since no measurements could be done with helium in the laboratory, a comparison analogous to that of the previous section is not possible. Therefore, all following results are to be taken with some skepticism.

5.2.1 Magnet temperature using only helium

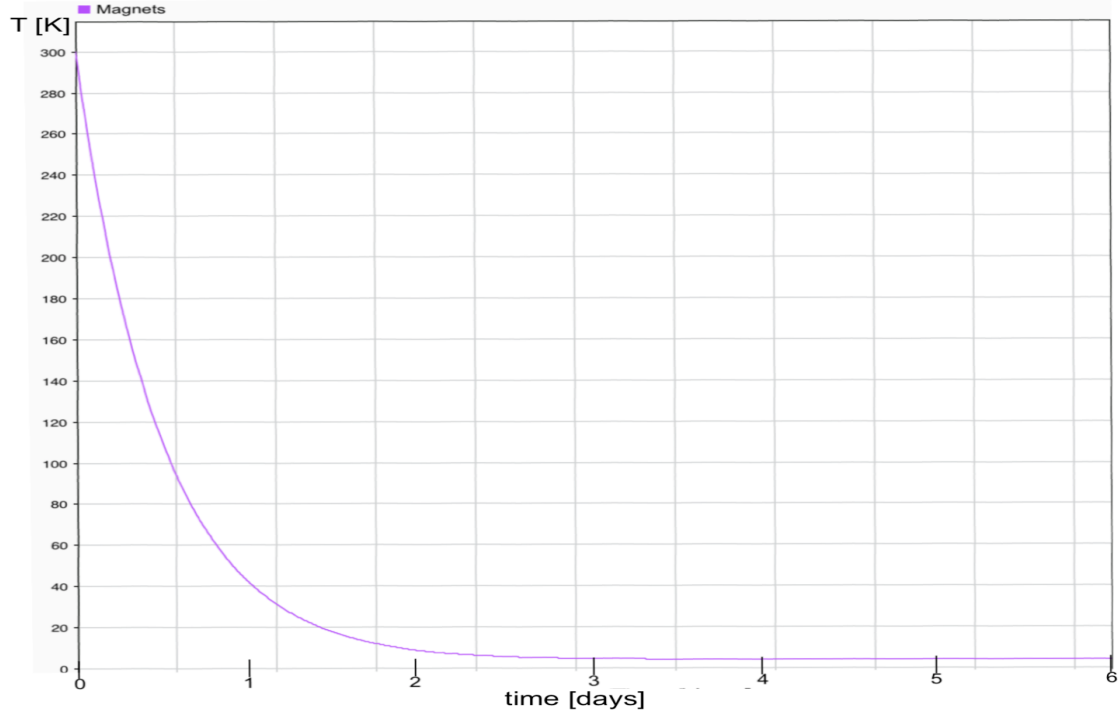


Fig. 34: Average magnet temperature with a helium flow of 8 g/s and no nitrogen flow. It takes 101.6 hours for the magnet to reach 4.2K.

Without the use of nitrogen, a helium flow of at least 8 g/s is necessary to decrease the temperature low enough for sufficient liquid helium to condense to cover the quench protection. Any lower than that, and the liquid level converges at an earlier point (see appendix H).

Figure 34 shows the temperature of the magnets for the case a helium flow of 8 g/s. The corresponding helium liquid level is shown in figure 35. When the magnet reaches temperatures close to 4 K, helium will start to condense at a maximum rate of 6.77 ml/s \equiv 0.845mg/s. The regulation function ensures that the liquid level remains barely above the 78.4%. The evaporation rate at minimal temperature is 93 mg/s or 522 ml/s of gaseous helium.

Under ideal circumstances (no exterior heat flow), the total mass of helium needed to cool down the magnets and the helium container to 4.2 K would be 327.8 kg (see appendix I). The simulation however reports a helium mass of 2926 kg. Due to the heat flow form the exterior, it is to be expected that the actual value is signifantly higher. However, this difference is substancial and likely unrealistic. Further measurements need to be done to confirm or deny this result.

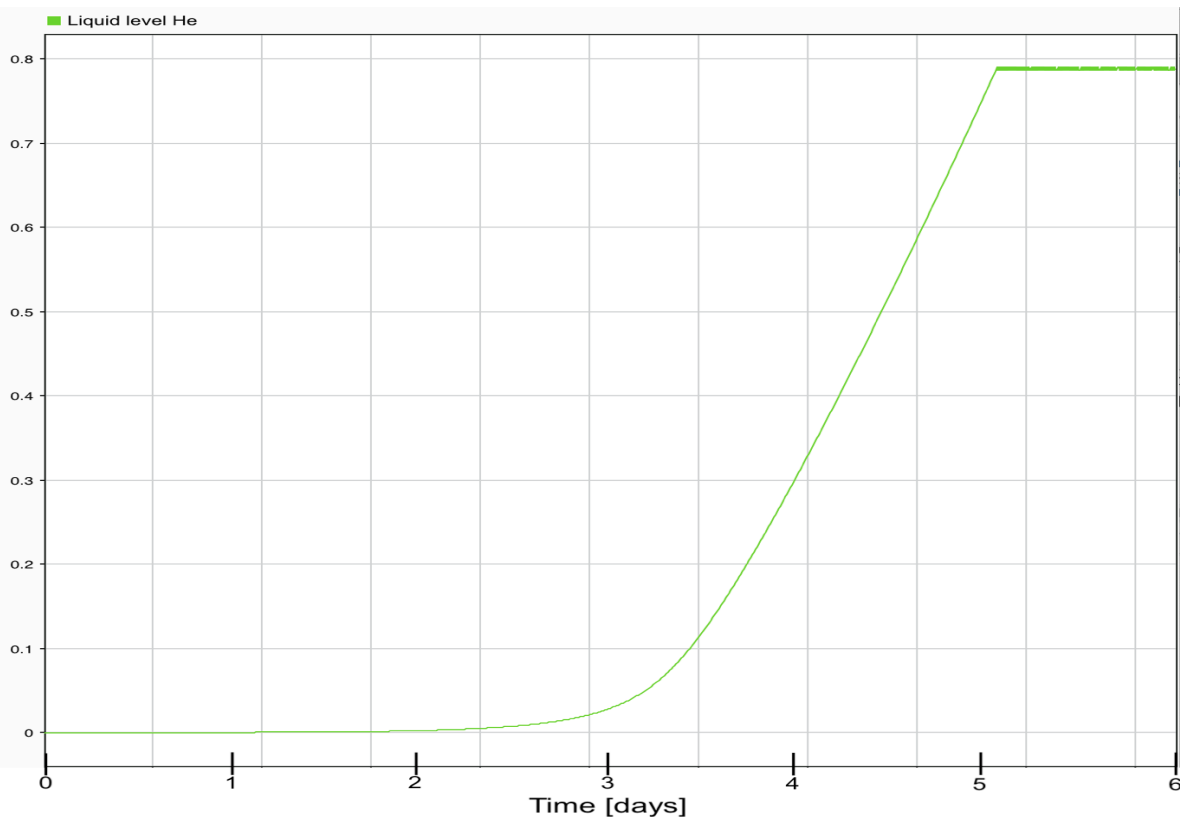


Fig. 35: Helium liquid level with a helium flow $8 \frac{\text{g}}{\text{s}}$ and no nitrogen flow.

5.2.2 Magnet temperature using helium and nitrogen

With the colder shield, the heat flow to the helium container is decreased. When additional cooling with nitrogen takes place, a smaller helium flow of 6 g/s is sufficient.

No pre-cooling: First, we will examine the results in the case of a simultaneous initiation of the helium and nitrogen flow (see figure 36).

When the magnet reaches 4.2 K, 2382kg of helium has been used. This is 18.6 % less than in the case of no nitrogen flow.

Out of interest, an MLI sheet was added on the outer side of the helium container in the simulation. This reduced the cooling time by about 1.5 hours.

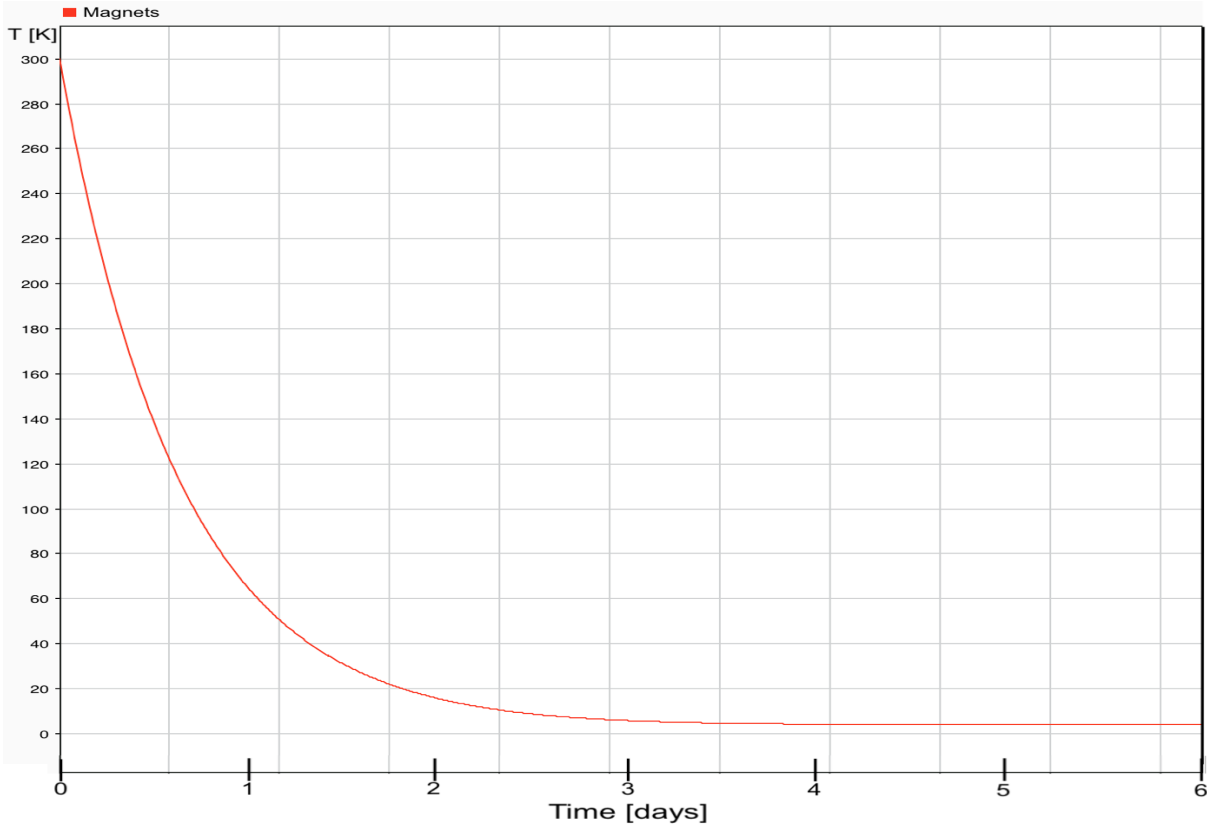


Fig. 36: Average magnet temperature with a helium flow of $6\frac{\text{g}}{\text{s}}$ and simultaneous initiation with the nitrogen flow. It takes 110.3 hours for the magnet to reach 4.2 K after initiating the helium flow.

With pre-cooling: Figure 37 shows the behaviour of the magnet temperature if the helium flow is activated only when the shield reaches minimal temperature (at $t \approx 1.6$ days). 2247 kg of liquid helium is needed to cool the magnet to minimal temperature. This is 5.66 % percent less compared to before, and 23.2% percent less than in the case of not using nitrogen at all.

If the helium flow is 8g/s, it only takes 60.0 hours to cool the magnet, which is about 41 % percent shorter than in the case of no nitrogen use.

The evaporation rate at minimal magnet temperature is 74 mg/s or 415ml/s of gaseous helium, which is about 20.5 % less than in the case of an uncooled nitrogen shield.

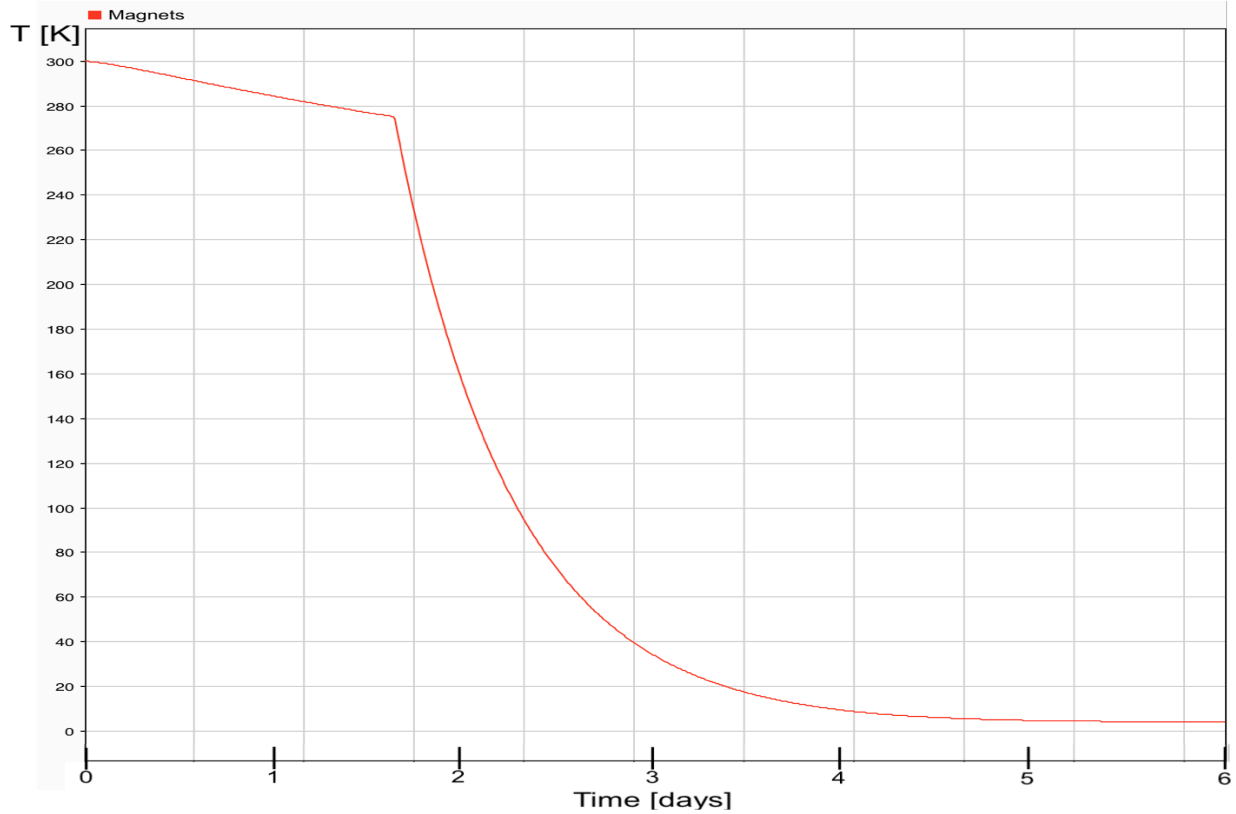


Fig. 37: Average magnet temperature with a helium flow of $6 \frac{\text{g}}{\text{s}}$ and initiation after the shield reaches 80 K. It takes 103.9 hours for the magnet to reach 4.2 K after initiating the helium flow.

With a helium price of 25 €/l \equiv 200€/kg, the total cost of helium needed to cool down the magnets in the case of pre-cooling with nitrogen would be about 450000 €. However, the used helium is not wasted but instead re-liquified. Therefore, the actual amount of helium needed depends on the liquification rate.

For an overview of the results of this chapter, see tabular 2.

Tab. 2: Comparison of cooling time and helium use until magnets reach 4.2 K.

Process	Time [h]	Used helium [kg]
Only helium (higher flow)	101.6	2926
Helium and nitrogen simultaneously	108.3	2382
Helium when shield reaches 80 K	103.9	2247

6 Conclusion and outlook

Because of the mentioned issues regarding the setup, a full conclusion on the accuracy of the simulation cannot be drawn. However, some early indications can be discerned:

Qualitatively, the simulation provides good results. We were able to determine that a continuous liquid nitrogen flow of 10 l/s would be sufficient to cool the shield down to minimal temperature within 16 hours.

However, the quantitative disagreement between the simulation results and the measured temperatures is significant (up to 34K). This is mainly due to the fact that the simulation does not take the varying nitrogen flow rate into account.

Under the assumption that the simulation involving helium is accurate, we were able to discern that a flow of 6 g/s is sufficient to cool down the magnets to minimal temperature. At thermal equilibrium, the simulation reported an evaporation rate of 74 mg/s. This would entail that a helium flow no less than this is necessary to maintain minimum magnet temperature. The simulation results also allowed us to find out that pre-cooling the assembly reduces helium use by 5.66% compared to cooling with liquid helium and nitrogen simultaneously.

Whether or not any of these values are realistic, remains up for question until the cooling with helium is available in the experiment.

Bearing in mind the additional work done in the laboratory to set up the experiment as well as the time it took to become familiar with the program, the development of a more detailed model representing quantitative measurements was not possible. However, it is feasible to build on the existing model, taking into the account the non-constant nitrogen flow and creating more extensive thermal mass systems that represent the dimensions of each component.

From the measurements themselves, we can certainly conclude that a nitrogen setup less provisional than ours will be necessary for the actual neutron lifetime experiment.

Appendices

A Calculation of the magnet mass

The weight of the stainless steel housing was given to be 2250 kg. A 2.25 meter long sample of the superconducting wire was provided and measured to weigh 10.0 g. This gives a length density of $4.464 \frac{\text{g}}{\text{m}}$. Therefore, the used 72345 m of wire weighs $4.646 \frac{\text{g}}{\text{m}} \cdot 72345\text{m} \approx 336\text{kg}$. Combined with the weight of the housing, we yield 2586 kg for the total weight of the magnets. From the CAD model, it was estimated that the inner magnet shares 19% of the total mass, which gives us 491 kg for the inner magnet and 2095 kg for the outer and bottom magnets.

B Example simulations to demonstrate the influence of the isolation vacuum and the inclusion of MLI

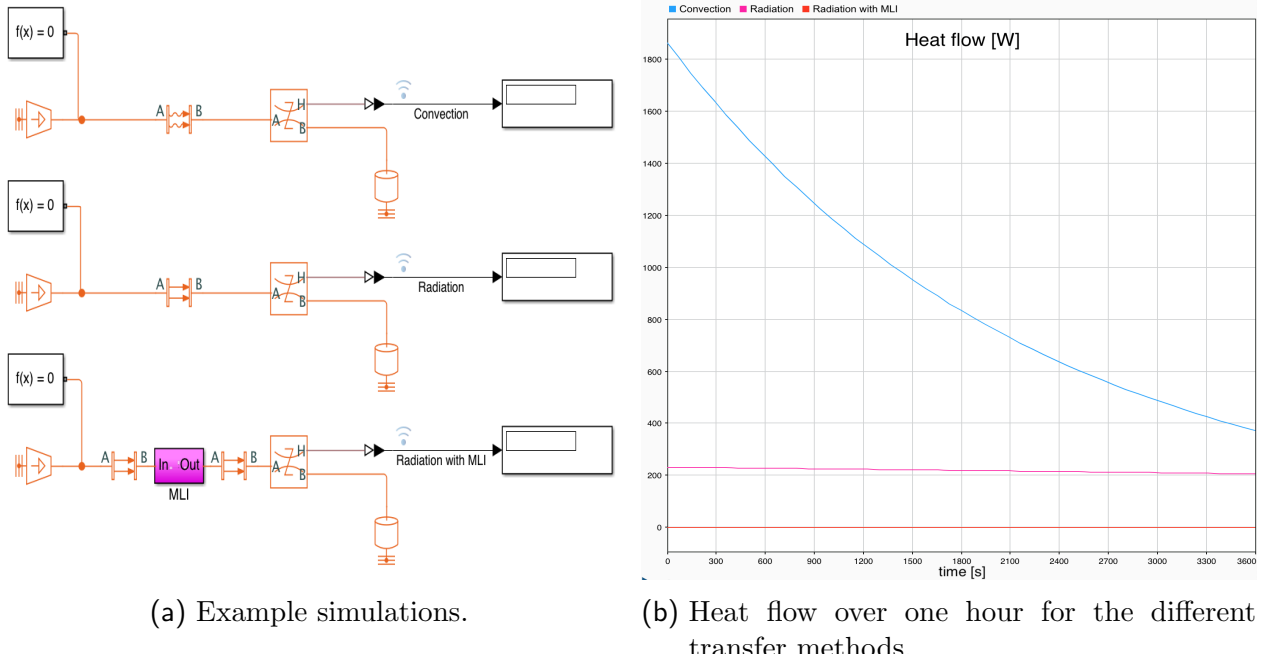


Fig. 38: Demonstration of the efficacy of the isolation vacuum and Multi-layer Insulation by means of some simple simulations.

Figure 38a depicts three different simulations. The constant temperature source is set to 293 K, while the mass has an initial temperature of 200 K. The heat transfer blocks have an area

of 1 m^2 each. The convective heat transfer coefficient is set to $20 \frac{\text{W}}{\text{m}^2\text{K}}$ (air, free convection [13]). The Multi-layer Insulation in the bottom simulation is assumed to have an emissivity of 0.003, like in the main simulation. The temperature sources and the thermal masses are assumed to be black bodies, maximizing radiative heat flow.

As you can see in figure 38b, the initial heat flow by means of convection is greater to that through radiation by about an order of magnitude. The difference in the heat flow from radiation to convection decreases over time solely due to the fact that the temperature gradient decreases much faster in the case of convection. The heat flow to the mass with the added MLI is $\sim 0 \text{ W}$.

C Non-simplified simulation involving only liquid nitrogen

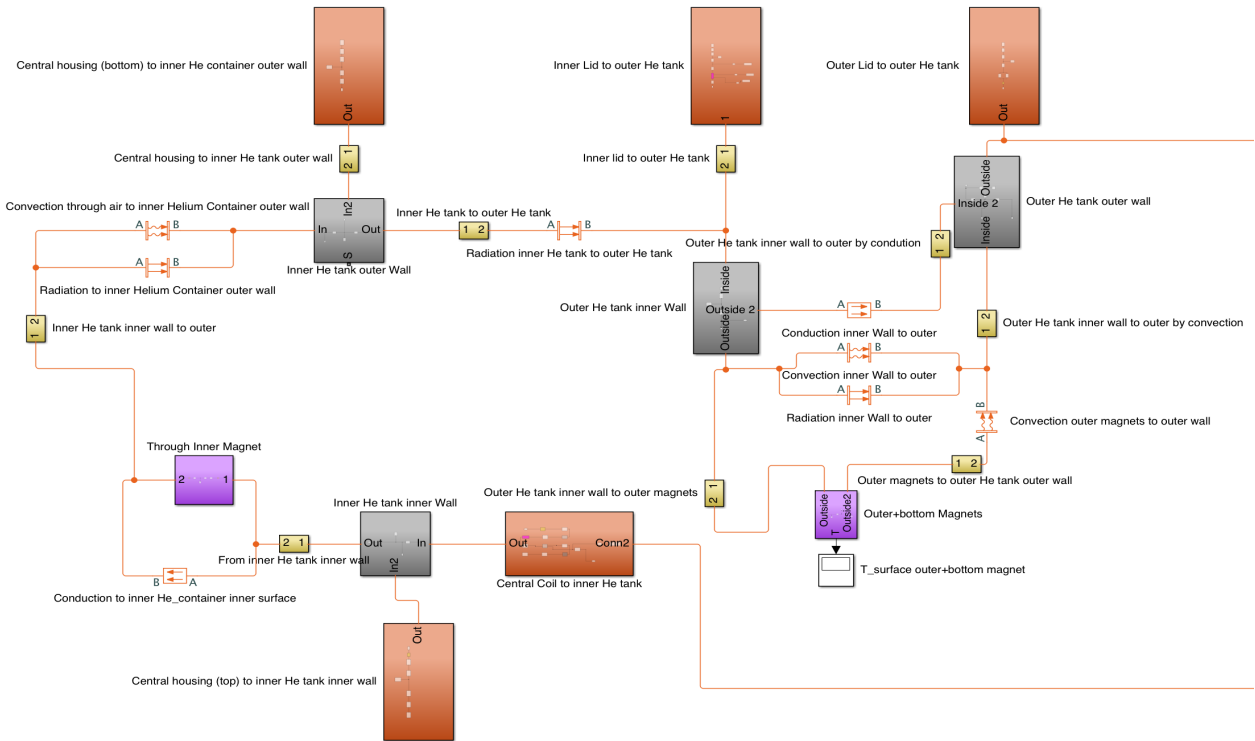


Fig. 39: Thermal simulation involving the air-filled helium tank and magnets

Figure 39 shows the part of the simulation that differs from the main simulation. In it, you can see that the space between each of the walls of the inner and outer helium container is thermally bridged by convective and radiative heat transfer blocks, representing the air in

the container. Note that the lines leaving this part of the simulation connect to the lines of the other part of the simulation. This other part is identical to that in the main simulation shown figure 12.

D Justification for only examining the simplified simulation

Note that the general simulation only represents a simplification when there is no helium involved.

The significant difference of the two simulations is that - in the main simulation - the outer walls of the helium container have the same temperature as the inner walls and magnets (same connection to the Receiver Accumulator in figure 40a). As mentioned in section 4.2, this is inevitable because of the way the Receiver Accumulator functions.

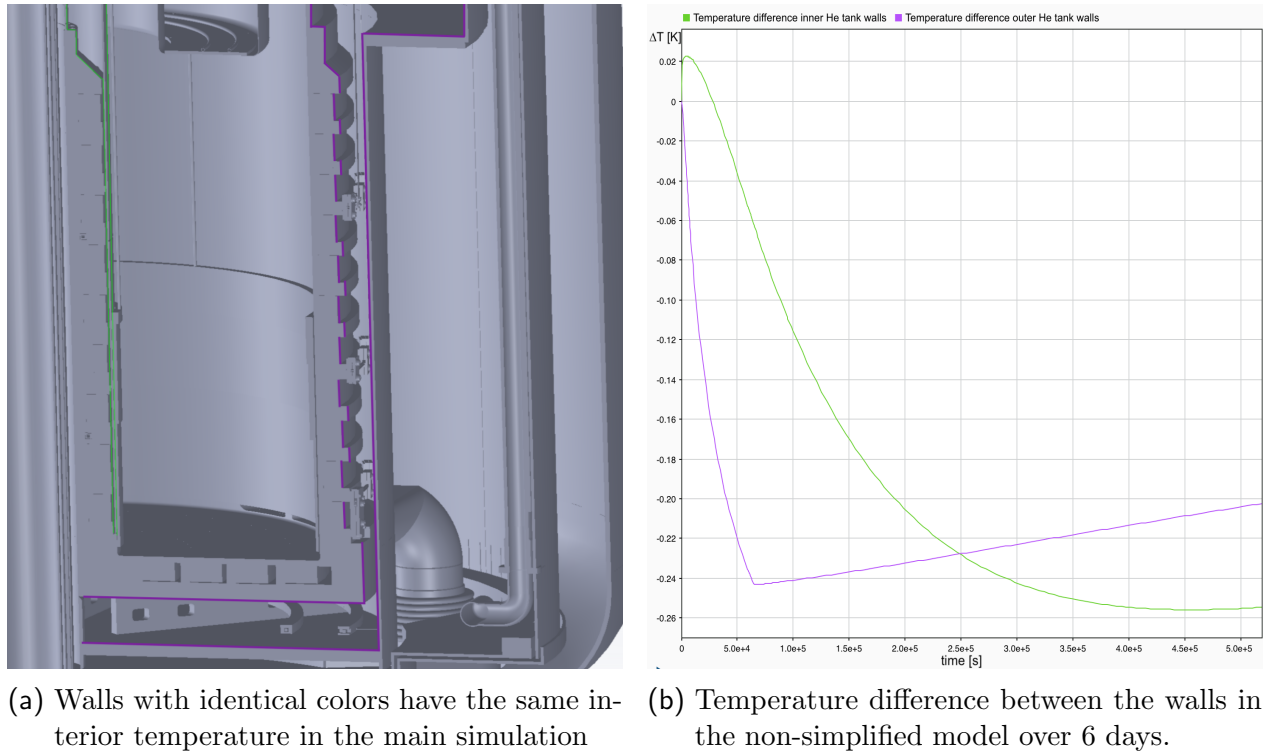


Fig. 40: Temperature differences of the walls

Let us examine how significant this simplification is when the helium tank is filled with air.

For this, we can compare the temperatures of facing walls in the non-simplified simulation (see figure 40b). As you can see, the temperature difference never exceed 0.25 K. Therefore, it is reasonable to only regard the main model, even when analyzing the results where no helium is used.

E Dimensions of components as used in the simulation

The following values are obtained through the CAD model in Solidworks®. Tabular 3 shows dimensions of the central assembly.

Tab. 3: Dimensions of components of the central assembly

Component	Area	Thickness	Material
Inner Magnets	0.91 m ²	39.7 mm	Stainless Steel, Copper, NbTi and FORMVAR insulation
Bottom Magnets	0.71 m ²	71.0 mm	— " —
Outer Magnets	2.27 m ²	39.7 mm	— " —
Central Coil	0.62 m ²	9cm (Diameter)	Copper

Tabular 4 shows dimensions involving the helium container.

Tab. 4: Dimensions of components of the helium tank

Component	Area	Thickness	Material
Inner part inner wall	0.86 m ²	3 mm	Stainless steel
Inner part outer wall	1.50 m ²	3 mm	— " —
Outer part inner wall	4.05 m ²	8 mm	— " —
Lid	1.00 m ²	30 mm	— " —
Outer cylindrical parts	6.84 m ²	6 mm	— " —
Outer parallel parts	1.85 m ²	20 mm	— " —

Tabular 5 shows the measurements of the connections leading to the helium container. Note that here, the area is the cross-sectional area through which heat can travel from the lid to the tank. The effective length of connections with corrugations is estimated. The mountings are assumed as cylinders.

Tab. 5: Dimensions of connections to the helium tank (corrugations included)

Component	Area	(effective) Length	Material
Mountings (6x)	6.16 cm ²	60 cm	Titanium
He-Inlet	0.5 cm ²	80 cm	Stainless steel
He-Outlet	45 cm ²	80 cm	— ” —
Liquid level sensor connections (3x)	1.4 cm ²	60 cm	— ” —
Power supply connections (2x)	4 cm ²	60 cm	— ” —
Temperature sensor cable entry	6.7 cm ²	45 cm	— ” —

Tabular 6 shows some important dimensions of the shield and mountings, while tabular 7 shows those of the nitrogen pipes.

Tab. 6: Dimensions of the shield and mountings, and lid connection (corrugations included)

Component	Area	Thickness	Material
Mountings (6x)	6.16 cm ²	40 cm (length)	Titanium
Direct connection	17.16 ²	35 (length)	Stainless steel
Shield lid	1.47 m ²	2 mm	Aluminum
Shield sides	10.3 m ²	3 mm	— ” —
Shield bottom	2.4 m ²	5 mm	— ” —

Tab. 7: Dimensions of the nitrogen pipes

Component	Outer Area	Thickness	Inner diameter	Length	Material
Inner pipes (vertical)	0.83 m ²	2 mm	20 mm	664 cm	Aluminum
Inner pipes (axial)	0.56 m ²	2 mm	20 mm	440 cm	— ” —
Outer pipes	0.72 m ²	2 mm	20 mm	440 cm	— ” —

Tabular 8 shows the dimensions of all parts directly in contact with the exterior.

Tab. 8: Dimensions of the outer parts

Component	Area [m ²]	Thickness [mm]	Material
Outer wall	15.71	8	Stainless Steel
Inner lid	0.88	57	— " —
Outer lid	2.30	57	— " —
Central housing (bottom)	0.19	5	— " —
Central housing (top)	0.14	4	— " —

Tabular 9 shows the material constants used in the simulation. Note that the coefficients are temperature dependend, but constant values for all different temperatures needed to be assumed.

Tab. 9: Coefficients and specific heat capacities of the materials. " / " implies that the value is irrelevant in the simulation

Material	Specific heat [$\frac{\text{J}}{\text{kgK}}$]	Conductive [$\frac{\text{W}}{\text{mK}}$]	Emissivity	Convective [$\frac{\text{W}}{\text{m}^2\text{K}}$]
Air to steel	/		/	20 [13]
Stainless steel	447 [14]	20 [15]	0.2 [16]	/
Aluminum	900 [17]	237 [18]	0.09 [19]	/
Magnet (weighted avg.)	452 [14] [17] [20] [21]	23.3 [13] [20] [18] [15]	/	/
MLI	225 (assumed 1/4 Al)	10 [22]	0.003 (est.)	/
Armaflex	/	0.034[23]	/	/

F Calculation of the liquid level necessary to cover the quench protection

The liquid level that would be measured in the experiment would be 142 cm or 89.3%, since the total height of the helium container is 159 cm. However, the liquid level that the Receiver Accumulator measures consists of the volume fraction rather than the height fraction, since it resembles a container with a homogeneous area for every height. Therefore, the liquid level

that would cover the quench protection in the simulation is

$$\text{LL} = \frac{655 \text{ l (Volume up to quench protection)}}{835 \text{ l (total volume)}} = 78,4\%. \quad (10)$$

G Sensor descriptions

Tab. 10: Descripton of sensor positions and type [24]

Number	Position	Type
1	IC 10-	Cernox
2	IC 10-	Cernox
3	IC 12-	Cernox
4	IC 12-	Cernox
5	IC 14-	Cernox
6	IC 14-	Cernox
7	OC 22+	Cernox
8	OC 22+	Cernox
9	OC 18-	Cernox
10	OC 18-	Cernox
11	OC 27+	Cernox
12	OC 27+	Cernox
13	Helium tank: Coil domain	PT100
14	Helium tank: Coil domain	PT100
15	Helium tank: Coil domain	PT100
16	Helium tank: Coil domain	PT100
17	Inner shield	PT100
18	Inner shield	PT100
19	Inner shield	PT100
20	Inner shield	PT100
21	Shield: floor	PT100
22	Shield: floor	PT100
23	Shield: outer part	PT100
24	Shield: outer part	PT100
25	Shield: lid	PT100
26	Shield: lid	PT100
27	Central MLI	PT100
28	Central MLI	PT100
29	Central MLI	PT100
30	Central MLI	PT100
31	Inner lid: Inside	PT100
32	Inner lid: Inside	PT100

H Liquid level in the case of an insufficient helium flow rate

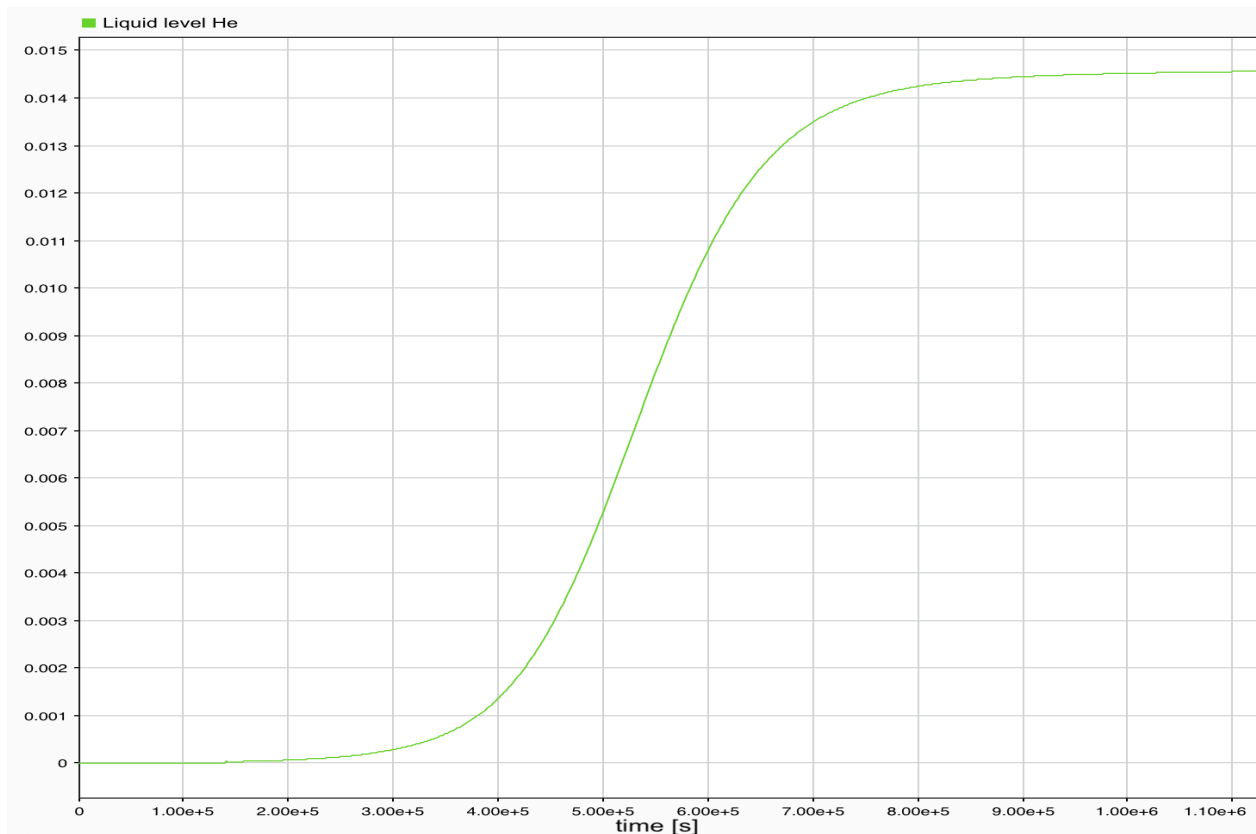


Fig. 41: Helium liquid level in the case of an insufficient helium flow over 13 days

If the helium flow is too low, the liquid level will converge at a lower point than 0.784 (see figure 41).

I Calculation of the helium mass needed to cool down the magnet under ideal circumstances

If there is no exterior heat flow and the all helium is used just to cool the magnets, the amount needed can be easily calculated. The energy the helium receives is then equal to the heat that the magnet loses:

$$\Delta q_{\text{He}} \cdot m_{\text{He}} = c_p \cdot m_{\text{magnets}} \cdot \Delta T. \quad (11)$$

Here, Δq_{He} denotes the enthalpy difference of gaseous helium at room temperature to that of liquid helium. $c_p = 452 \frac{\text{J}}{\text{kg K}}$ is the specific heat of the magnet (weighted average of all components) and $\Delta T = 293 \text{ K} - 4.2 \text{ K} = 288.8 \text{ K}$ is the temperature difference of the magnets. The latent heat of helium is 21 kJ/kg [25] (smaller than that of nitrogen by a factor of 10 [26]). The enthalpy difference of helium gas at room temperature and liquid helium temperatures is of about 1.5 MJ/kg [25]. Therefore, Δq_{He} is equal to 1.521 MJ/kg.

Solving for m_{He} and using the calculated magnet mass of 2583 kg, we yield $m_{\text{He}} = 221.7 \text{ kg}$.

Since the helium container will also be cooled down, additional helium is needed even without any exterior heat. With the specific heat of stainless steel being $447 \frac{\text{kJ}}{\text{kg K}}$ [14] and with a total weight of 1250 kg, an additional 106.1 kg of helium is required.

Therefore, the total mass of helium needed to cool down all components that it comes in direct contact with is 327.8 kg.

References

- [1] Z. Charifoulline, “Residual Resistivity Ratio (RRR) Measurements of lhc superconducting nbt_{1-x} cable strands,” 2006.
- [2] G. L. Greene and P. Geltonbort, “The Neutron Enigma,” *Scientific American*, 2016.
- [3] “Neutron Lifetime Measurement Using a Cold Neutron Beam.” <https://www.nist.gov/programs-projects/neutron-lifetime-measurement-using-cold-neutron-beam>, 14-08-2015. Accessed: 12-08-2020.
- [4] S. Paul, “The Puzzle of Neutron Lifetime,” Technische Universität München, 3 2009.
- [5] “Wärmeleitung.” <https://de.wikipedia.org/wiki/Wärmeleitung>. Accessed: 15-08-2020.
- [6] D.-L. Liu, “Particle Deposition onto Enclosure Surfaces,” *Developments in Surface Contamination and Cleaning: Particle Deposition, Control and Removal*, 2010.
- [7] A. J. N. Khalif and I. R. A. Al mousawi, “Comparison of Heat Transfer Coefficients in Free and Forced Convection using Circular Annular Finned Tubes,” 2016.
- [8] E. Generalic, “Blackbody radiation.” <https://glossary.periodni.com/glossary.php?en=blackbody+radiation>, 20-10-2018. Accessed: 17-08-2020.
- [9] L. Smith, “The ABCs of Multi-Layer Insulation for Spacecraft.” <https://www.designnews.com/materials-assembly/abcs-multi-layer-insulation-spacecraft>, 2019. Accessed: 22-08-2020.
- [10] “Multi-layer Insulation.” https://en.wikipedia.org/wiki/Multi-layer_insulation. Accessed: 22-08-2020.
- [11] “Multi-layer Insulation (MLI).” <https://bit.ly/34EDDaD>. Accessed: 24-08-2020.
- [12] J. M. Pendlebury and K. Smith, “The Electric and Magnetic Moments of the Neutron,” *Philosophical Transactions of the Royal Society of London. Series B, Biological Sciences*, vol. 290, 1980.
- [13] Engineeringtoolbox.com, “Overall Heat Transfer Coefficient.” <https://bit.ly/2SFeyqy>. Accessed: 20-08-2020.

- [14] Engineersedge.com, “Specific Heat Capacity of Metals Table Chart.” https://www.engineersedge.com/materials/specific_heat_capacity_of_metals_13259.htm. Accessed: 30-08-2020.
- [15] H. Recknagel, *Taschenbuch für Heizung + Klimatechnik*. Vulkan-Verlag GmbH, 2016.
- [16] Engineeringtoolbox.com, “Emissivity Coefficients Materials.” https://www.engineeringtoolbox.com/emissivity-coefficients-d_447.html. Accessed: 15-09-2020.
- [17] Ucdsb.on.ca, “Specific Heat Capacity Table.” http://www2.ucdsb.on.ca/tiss/stretton/database/Specific_Heat_Capacity_Table.html. Accessed: 30-08-2020.
- [18] Engineeringtoolbox.com, “Thermal Conductivity of Metals, Metallic Elements and Alloys.” https://www.engineeringtoolbox.com/thermal-conductivity-metals-d_858.html. Accessed: 30-08-2020.
- [19] “TABLE OF EMISSIVITY OF VARIOUS SURFACES.” https://www.transmetra.ch/images/transmetra_pdf/publikationen_literatur/pyrometrie-thermografie/emissivity_table.pdf. Accessed: 15-09-2020.
- [20] Periodictable.com, “Technical data for Niobium.” <https://periodictable.com/Elements/041/data.html>. Accessed: 09-09-2020.
- [21] Nuclear-power.net, “Titanium – Specific Heat, Latent Heat of Fusion, Latent Heat of Vaporization.” <https://bit.ly/3iRj281>, 2019. Accessed: 30-08-2020.
- [22] P. M. Sutheesh and A. Chollackal, “Thermal performance of multilayer insulation: A review,” 2009.
- [23] “Armaflex AC.” <http://armacell.com/WWW/armacell/INETArmacell.nsf/mobile/D6CBDA3F1E2D3301C12579EF0077E16C>. Accessed: 17-09-2020.
- [24] H. Hartmond, “Validierung des Vakuum- und LN2-Systems für das PENeLOPE Experiment,” Technische Universität München, 9 2020.
- [25] R. Álvarez Montoya, S. Delgado, J. C. J. Navarrete, N. DíazContreras, J. R. Marijuan, V. Barrena, I. Guillamón, and H. Suderow, “Methods to simplify cooling of liquid Helium cryostats,” 4 2019.

- [26] Nuclear-power.net, “Nitrogen – Specific Heat, Latent Heat of Fusion, Latent Heat of Vaporization.” <https://www.nuclear-power.net/nitrogen-specific-heat-latent-heat-vaporization-fusion/>, 2019. Accessed: 08-10-2020.